CARBON NANOMATERIALS AS IMAGING, SENSING, AND DELIVERY AGENTS FOR CANCER THERAPEUTICS

by

Elizabeth Campbell

Bachelor of Science in Physics May 2014

University of Dallas

Irving, Texas

Submitted to the Graduate Faculty of the

College of Science and Engineering

Texas Christian University

in partial fulfillment of the requirements

for the degree of

Master of Science

December 2018

ACKNOWLEDGEMENTS

Lastly, I am beyond thankful to my mother, sisters, friends, my husband Trent and my daughter Olivia for their unending support and encouragement to pursue my education at TCU.

TABLE OF CONTENTS

LIST OF FIGURES

LIST OF TABLES

LIST OF ABBREVIATIONS

GO – Graphene oxide

GQD – Graphene quantum dot

N-GQD – Nitrogen doped graphene quantum dot

NS-GQD – Sulfur doped graphene quantum dot

BN-GQD – Boron-nitrate doped graphene quantum dot

NIR – Near-infrared

AFM – Atomic force microscopy

SEM – Scanning electron microscopy

TEM- Transmission electron microscopy

CTCF – Corrected total cell fluorescence

CHAPTER- 1
BACKGROUND STUDY

1.1 Motivation

Graphene is utilized in a number of applications due to its unique properties, including high electrical[1] and thermal[2] conductivity, tensile strength[3] and transparency[4]. As graphene is insoluble in water and does not exhibit fluorescence, such applications are limited to passive platforms for sensing and cell work. Graphene derivatives, however, such as graphene oxide (GO) and graphene quantum dots (GQDs), possess unique properties which make them more attractive for biomedical applications: both are water soluble, provide a versatile platform with a variety of addends for convenient functionalization-based drug attachment, and both exhibit low to no cytotoxic response at concentrations used in our work. Additionally, many forms of GO and GQDs exhibit intrinsic fluorescence in the visible[5,6] and even in the near-infrared, which can be optimal for *in-vitro* and *in-vivo* imaging. These advantageous properties, as well as unique optical sensing capacity of GO and GQDs have not been fully utilized to date for biological applications. This study aims to fill this gap by exploring the properties of GO and GQDs as standalone multifunctional agents for imaging in visible/near-infrared, cellular internalization, and biosensing.

1.2 Questions to be Answered

i. Are graphene oxide and graphene quantum dots suitable for biomedical applications?

Here, we will study the properties of the material itself via size characterization, cytotoxicity, degradation of the material over time, and the emission spectra at varying pH levels. This will indicate if the material can be utilized as a multi-modal agent *in vitro*, and will be covered in chapter 2.

ii. Can these nanomaterials be used for imaging and delivery?

This question leads us to evaluate the ability of the material to be imaged and internalized in cells. We will determine the ideal imaging settings and detect emission from nanomaterials over cell autofluorescence background. We will also determine the timeline for cellular internalization and excretion for future drug/gene delivery. This analysis will be discussed in chapter 3.

iii. Do they offer sensing capabilities?

At this point in the study, we will be looking to see if the material can offer biosensing capabilities *in vitro*. Referencing the emission spectra at varying pH levels (discussed in chapter 2), we will determine if the nanomaterials can be used as nanoscale sensors of intra- and extracellular pH in chapter 4.

1.3 Introduction

Cancer is one of the leading causes of death worldwide, with a staggering estimated death toll of over 609,000 in the United States alone in 2018[7]. While existing therapies such as radiation, and chemotherapy can be successful[8], they often affect both healthy and cancer tissues, which can be detrimental to patients' health. Current cancer chemotherapies are not deterministic and offer little information about the treatment pathways. Thus, very important developments arise in the area of image-guided therapies[9] utilizing fluorescent dyes and nanomaterial platforms for therapeutic tracking that can also improve cancer survival rates, detect cancer, and explain treatment pathways. Fluorescence is an optical effect that is utilized to track the material in the biological cells and tissues. The fluorescence process in materials involves excitation of an electron over a band gap into an excited state after which it decays into a lower, valence band allowed state and its energy is released in the form of a photon that has generally lower energy than the excitation photon. Fluorescence is used in bio-applications in a variety of ways, including fluorescent dyes for bioimaging[10,11], fluorescence resonance energy transfer (FRET) allowing for the highly sensitive study of molecular interactions or distances between molecules in biological environments[12] enabled due to the energy transfer between a donor and acceptor fluorophore which is dependent on the inverse distance separating the two molecules to the sixth power[13], and two-photon excitation microscopy that allows using high penetration depth near-infrared photons to excite fluorescence dyes and nanomaterials deeper in the biological tissue [14].

Nanomaterials are on the forefront of being utilized for biomedical applications, including their use in treatment and detection of cancer[15], central nervous system (CNS) diseases[16], sickle cell[17], and autoimmune disorders[18]. They provide a platform that can be altered to address specific needs of the particular disease treatment and can be integrated into a system to either suppress or

stimulate desired traits, such as antitumor effects or treatment of inflammatory disorders[19,20]. They can also image treatment in cancer cells and tissues in the visible[21] and near-infrared (NIR)[22] and enable targeted delivery[23,24]. Drug delivery is beneficial as delivery agents may protect the healthy tissue from adverse effects of chemotherapeutics encapsulating them and it also enables safe transport of gene therapeutics prone to degradation and water-insoluble drugs to cancer tumor sites and cells. The power of nanotechnology-based systems lies in their multi-functionality, offering both drug delivery and detection capabilities.

The potential to perform multiple functions using one agent is the attractive force driving the integration of molecular therapeutics with nanomaterials-based drug or gene delivery vehicle systems. Although such nanoformulations significantly improve the capabilities of conventional therapeutics, there is still a challenge to expand the options for image- and sensing-guided therapy and advance targeting to cancer cells and/or multiple cell types. Currently, very few systems can carry out imaging, sensing, and delivery concurrently[25], while none are used in clinic due to low biocompatibility[26], complex fabrication[27], lack of in-vivo imaging and detection capabilities, issues with body clearance[26], and unknown decomposition routes[28] unless otherwise altered. Biocompatible nanomaterials exhibiting environment-dependent electronic and/or structural properties are expected to fill this gap with a promise of utilization as molecular sensors as well as for imaging and drug delivery.

Most popular nanomaterial platforms, liposomes[26], polymers[29], quantum dots[30] and gold nanoparticles[26] seldom address all of these issues focusing more on just a few of the aforementioned functions. A new promising class of materials, including carbon-based platforms, has a potential to address near-infrared (NIR) imaging beneficial for *in vivo* work and non-toxic gene delivery[31]. Near-infrared imaging is significantly more suitable for in-vivo application than

that in visible exhibited by conventional dyes, as near-infrared light penetrates substantially deeper into biological tissue. However, cancer detection capabilities and potential toxicity issues of these materials still remain unaddressed. Graphene is yet another remarkable carbon material that is used in a variety of applications, ranging from water desalination[32] to new age electronics[33,34] graphene-assisted laser desorption/ionization for mass spectrometry[35] and high resolution electron microscopy[36]. Recently graphene has been used in biomedical applications including DNA sequencing[37], biosensor development[38], and graphene-enhanced cell differentiation and growth[38]. However, its insolubility in water leading also to asbestos-like toxicity and lack of band gap fluorescence hamper its use in bio-applications. Graphene derivatives[39,40] on the other hand including graphene quantum dots, graphene oxide[41] and an assortment of graphene-based nanoparticles[42,43] provide water-soluble platforms that can be optimized for imaging and drug/gene therapeutic transport. So far these materials have been used for targeted delivery[44-46], imaging[45,46] and chemical sensing[47]. In many of these applications, however, carbon nanomaterials have to be modified, via PEG conjugation for imaging, biocompatibility and therapy[48,49] or require the use of additional dyes for detection[50,51,52]. Such multicomponent formulations still may exhibit significant non-specific toxicity[44-46] due to some of their constituents, can be complex to reproducibly fabricate, and require external fluorophores for fluorescence tracking[53,54] while many of them also do not possess desired capabilities for cancer detection.

To date, we explored graphene oxide (GO) as a multimodal platform to address these issues[41]. Graphene oxide possesses unique properties which make it more attractive for biomedical applications: it is water soluble, provides a large platform with a variety of addends for convenient functionalization-based drug attachment, and exhibits fluorescence in visible/near-infrared. These properties are utilized in GO field-effect transistor biosensors [55, 56, 57], cellular probing and real-

time monitoring using a wide-field fluorescence microscope[58], and scaffolding for cell cultures and tissue engineering[59]. Finally, nanoscale graphene oxide has been adopted for the delivery of anticancer drugs into biological cells[55,60,61,62], as aptamers for ATP probing in mouse epithelial cells, and gene delivery[58,63,64]. For such applications, however, GO was modified and has only been utilized as a delivery agent or rarely as a fluorescence marker[59,61], requiring either incorporation of external fluorophores[50,65,66] or complementary covalent functionalization with PEG for successful delivery[66,67]. Additionally, many GO forms used in biological applications exhibit intrinsic fluorescence only in the visible[5,6] even with advantageous near-IR 2-photon excitation[68]. This can be optimal for *in vitro* work or low penetration depth imaging, but not for conventional *in vivo* studies where near-IR emission in the water window, where water absorption and tissue scattering are low, is desired for deep tissue penetration. All these complexities hamper the potential use of GO in biomedical applications resulting in the lack of data on its cytotoxicity and non-targeted intracellular accumulation. Finally, *in vitro* optical sensing capacity of GO has not been utilized to date. Our work fills this gap by exploring the properties of GO as a standalone multifunctional agent for imaging in red/near-IR, cellular internalization, and biosensing.

GO offers the benefit of a large platform for attachment of functional groups including targeting moieties, MRI agents and anticancer drugs[69], possesses imaging capabilities due to its fluorescence in the visible and NIR ranges, as well as pH-dependent electronic transitions[70]. pH-dependent emission is beneficial for optical cancer sensing as it offers the capabilities to detect a shift in the spectra depending on the environment. This is promising, as cancer environments are more acidic than healthy ones due excretion of lactic acid by cancer cells[71]. In this work, we explore the property of GO to vary its fluorescence as a function of pH[72] in the biological range for the detection of such cancerous environments. We suggest GO as a prospective platform for

therapeutics, as unlike other therapeutic nanoformulations, it can be produced at low cost and large quantities[73], and its oxygen-containing groups can be functionalized with molecular chemotherapy drugs in a variety of covalent and non-covalent approaches[74]. GO can also protect gene therapeutics from nuclease-mediated degradation[75,76,77], that is highly beneficial as we ultimately intend to utilize it for siRNA gene delivery. Additionally GO flakes developed and used in our work exhibit pH-dependent fluorescence in the red tailing into near-IR[72] spectral region with reduced biological autofluorescence background and tissue scattering. Here for the first time, we introduce a concept of *in vitro* optical pH sensing by GO and test the feasibility of GO as a novel multifunctional agent for delivery, imaging and sensing of cancerous environments.

Although GO has a high potential for multifunctional image-guided drug/gene delivery, its size, NIR imaging and some minor cytotoxicity limitations have a potential to be further addressed through utilizing zero-dimensional graphene quantum dots (GQDs). GQDs share desirable properties of graphene oxide including water solubility, and pH-dependent fluorescence, but also have a variety of attributes that can enhance their use in biomedical applications. Current applications of GQDs include their use as biological labels for stem cell research[52], cellular and deep tissue imaging[78], and photodynamic therapy[79]. GQD structures can be designed to exhibit higher quantum yields[80], stability against photo-bleaching[81], and few possess emission in the near-infrared[82]. NIR imaging modality has been hypothesized as a successful tool for *in vivo* imaging due to higher tissue penetration depth: as opposed to visible, NIR light can penetrate centimeters of biological tissue[83] allowing for *in vivo* fluorescence imaging for some targets.

GQDs fluorescing in the visible have already been utilized in a variety of biological applications including bioimaging[84]. The current obstacles with further utilizing these platforms for translational studies include complexity in preparation (widespread top-down approaches

provide poor reproducibility[85] while bottom-up approach tends to produce QDs with lower quantum yields[85]) and emission mostly in the visible[82]. Attempts to improve quantum yields[86] or facilitate NIR emission[87] typically increase QD toxicity due to the introduction of extra components or toxic functional addends. In order to address biocompatibility, complexity in fabrication and high-yield fluorescence capabilities along with near-IR imaging, we develop novel doped graphene quantum dots with advantageously modified optical properties. Nitrogen-doped (N-GQDs), sulfur-doped (NS-GQDs), and boron nitrate-doped (BN-GQDs) graphene quantum dots are synthesized via simplistic and reproducible 1-step hydrothermal route and tested for biological imaging both in visible and near-infrared as well as pH-based cancer detection *in vitro*. These GQDs demonstrating high biocompatibility, and high-yield visible emission along with near-IR fluorescence in NIR window I (650-950nm) show the capacity to become non-toxic standalone multifunctional agents for imaging in the visible and near-IR, effective cellular internalization, and biosensing.

CHAPTER- 2

SYNTHESIS AND CHARACTERIZATION OF NANOMATERIALS

2.1 Graphene Oxide

2.1.1 Fluorescence

Graphene oxide is a 2-D material derived from graphene by introducing oxygen functionalities, enabling fluorescence emission from GO that is not observed for graphene. Fluorescence of graphene oxide can be explained by two potential sources. The first theory contributes fluorescence origins to the islands of graphitic carbon surrounded by oxygen-based functional groups[88], and the second assumes that it originates from regions of confined electrostatic potential surrounding the functional groups[89,90]. Each theory can be explained using the quantum mechanical example of a particle in a box, such that we see the splitting of the energy levels and therefore, the creation of the bandgap in otherwise gapless graphene, which is derived from a smaller size of the confined region. Using the first theory, it can be explained such that the confinement of the graphitic regions impacts the free electrons within graphitic islands, causing the quantization of the energy levels. Due to confinement, the gap between the conduction and valence bands is introduced with the energy of several eVs yielding the possibility of fluorescence in the visible[88]. The second theory also resembles the 2D particle in a box example, in which, a confined region of electrostatic potential is considered around certain functional groups and is thought to be inducing electronic confinement. As we expect both the regions of graphitic carbon and regions of electrostatic potential vary in size across GO platform, GO fluorescence feature is expected to consist of multiple emission peaks with different emission energies. It is important to note, however, that neither of these theories for the pathways of GO emission have been fully confirmed although experimental evidence in ozone-driven oxidation of GO[91] points to the

possibility of manipulation of the size of graphitic regions that leads to change in fluorescence emission energies. GO is reported to fluoresce in the visible and tails into the near-IR[92] and can be seen in Figure 1a, which suggests it is beneficial for biological imaging. This is because there is less scattering of the light, which leads to the preferential transmission of longer wavelengths[83].
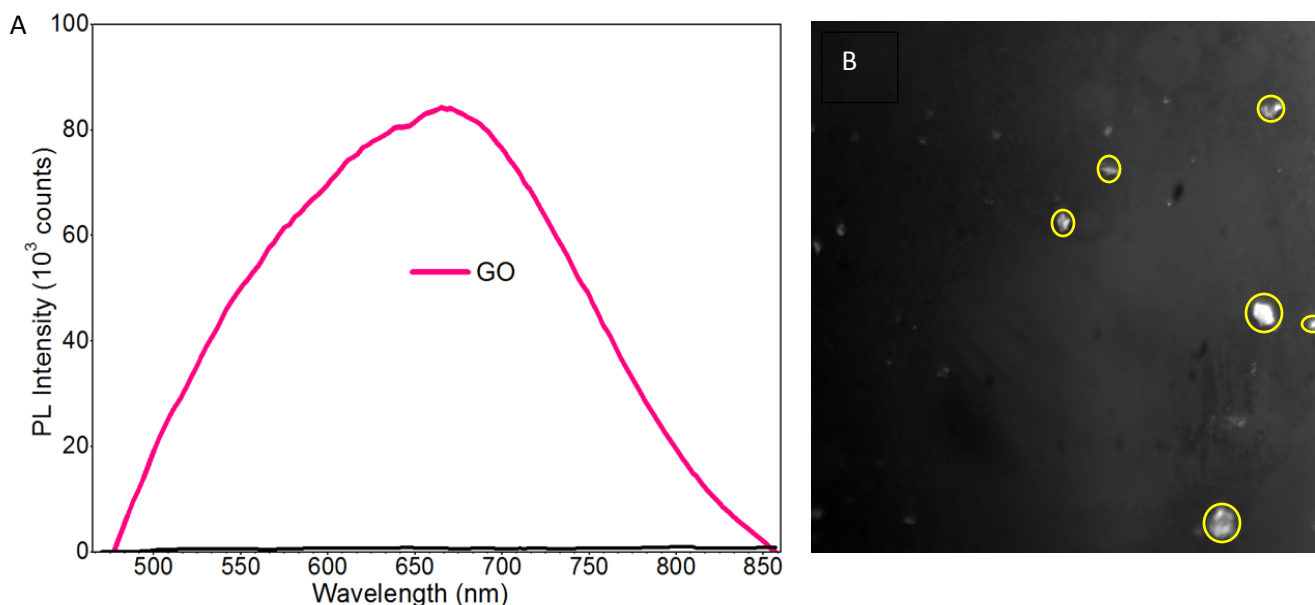
Figure 1 *A) Emission spectra for graphene oxide produced via the Hummers Method (different from our sample) in a very acidic environment. B) Circled GO flakes imaged at emission 650 nm.*

This allows for higher tissue penetration, up to a few centimeters[83], making graphene oxide an ideal material for its use in bioimaging applications. Additionally, GO flakes can be easily detected under the microscope (Figure 1b) and vary significantly in size which can be further adjusted by processing. This allows GO to be explored as a potential imaging agent for both *in vitro* and *in vivo* studies.

2.1.2 Size characterization

An advantage of GO as a delivery vehicle is its ease of modification, starting from the amount[93,94] and type[91] of functional groups to be explored in our further work, to the size of GO flakes[95]. To achieve optimal internalization and imaging conditions, we explore the influence of transfection time and the size of GO flakes on the internalization efficiency: generally, nanoparticle sizes below 200 nm, are expected to show improved cell penetration[96,97].

As GO flakes were purchased from commercial vendor, Gographene, initially GO flakes have a very broad distribution of sizes with high abundance in over 1μm flakes, which makes unprocessed GO unsuitable for cell internalization. In order to address that issue we began by varying the mean size of GO flakes by high power ultrasonic processing with a tip ultrasonicator at a 3W power setting for periods up to 60 minutes in aqueous suspensions. This processing dispersed GO in water and allowed for controllable size alteration of the flakes. As a result of that processing, flake dimensions (measured along their longest axis) decreased from approximately 1μm for non-treated GO down to 190 nm (Figure 2) with the expectation for small flakes, sized below 200 nm to show improved cell penetration[96,97]. The most extensive ultrasonic treatment (60 min), yielded substantial aggregation of GO flakes seen in SEM images (Figure 2-60 minutes), which is hypothesized to hamper successful internalization as the aggregates can range significantly in size or shape and also over time get combined with other aggregates and grow in size.
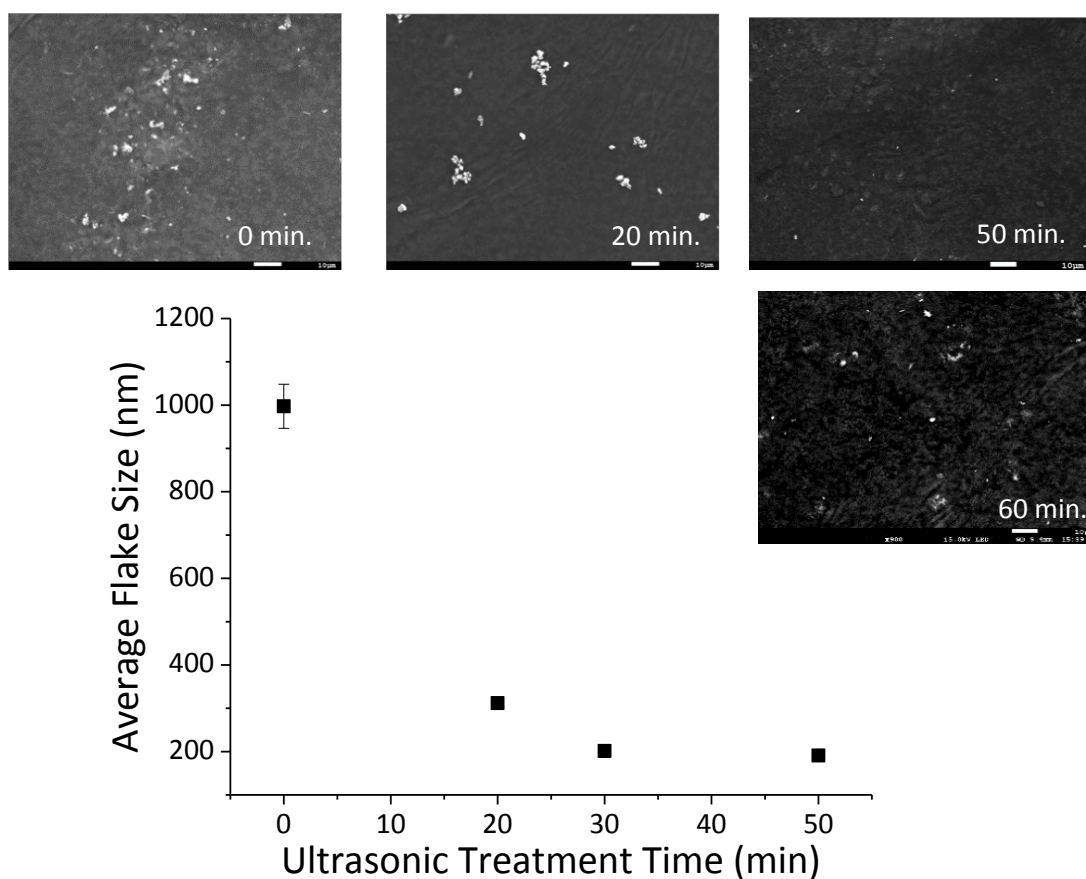
Figure 2 *Mean Flake Size vs. ultrasonic treatment time from SEM analysis. Error bars are below the size of some points. Insets are SEM images of GO flakes subject to 0 min to 60 min ultrasonic treatment. Scale bars are 10 um.*

Single-layer flake thickness identified in the atomic force microscopy (AFM) images provided by commercial GO supplier was verified by scanning electron microscopy (SEM) imaging (Figure 2) to ensure few-layered flakes so that the transverse flake dimensions are also compatible for successful internalization.
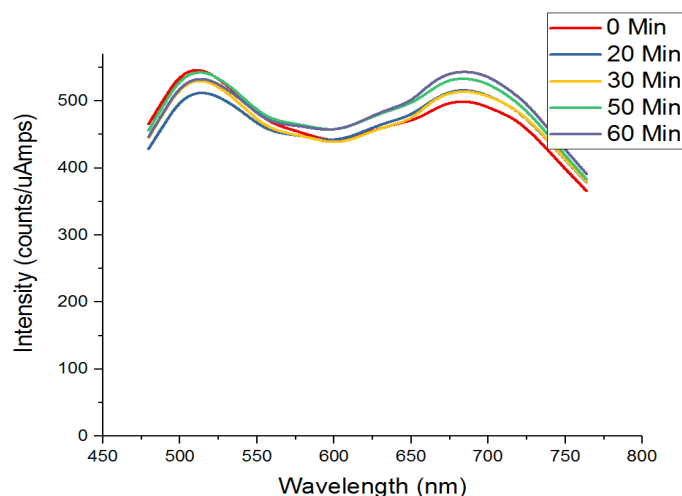
Figure 3 *Fluorescence spectra of varying ultra-sonication treatment procedures.*

This processing did not significantly affect GO fluorescence emission, therefore retaining its properties as an imaging agent (Figure 3).

2.1.3 Cytotoxicity

The issue of non-specific toxicity in healthy tissues is one of the major drawbacks for the use of nanomaterial-based platforms, preventing their translation into clinic. Other carbon platforms report large cytotoxic responses[98], which leads us to study the cell viability in the presence of graphene oxide. As opposed to the toxicity of water-insoluble carbon platforms[99], GO shows only small to negligible cytotoxic response with over 85% cell viability at the imaging concentrations of 15 µg/mL as indicated by the MTT assay (Figure 4), making it superior to many other carbon nanomaterials for biomedical applications. Expected concentrations for future patient use will likely depend on drug toxicity as opposed to GO toxicity. An MTT cytotoxicity assay is conducted using determined concentrations of the GO sample, Thiazolyl Blue Tetrazolium Bromide, and DMSO. Each sample is prepared via serial dilutions at the testing concentrations ranging from 0 to 15 µg/mL. The absorbance is measured using the FLUOstar Omega microplate reader, and analyzed using Omega software, where a higher absorbance is indicative of living cells.
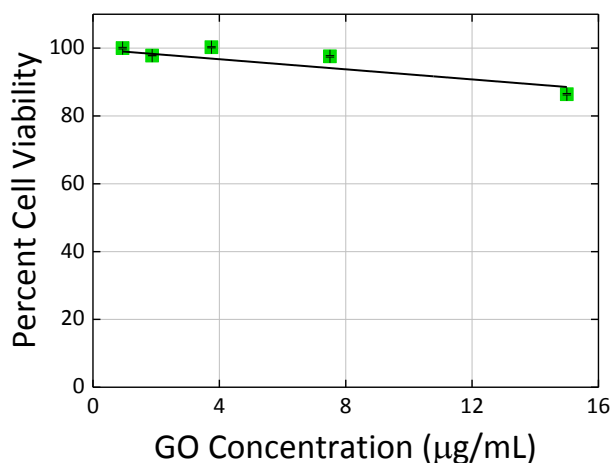
Figure 4 *Cytotoxicity of GO in HeLa cells showing percent cell viability with respect to the GO concentration (error bars are below the size of the points on the graph).*

2.1.4 pH dependent spectra

Since we envision GO as a multimodal agent for imaging, delivery, and sensing, we further explored its capabilities as a molecular pH sensor for cancer detection. This is allowed by pH-dependence of GO emission discovered in previous works[70,100] in the biological pH range with significant changes between pH 6 and 8 as seen from the fluorescence spectra of GO in suspension in (Figure 5).
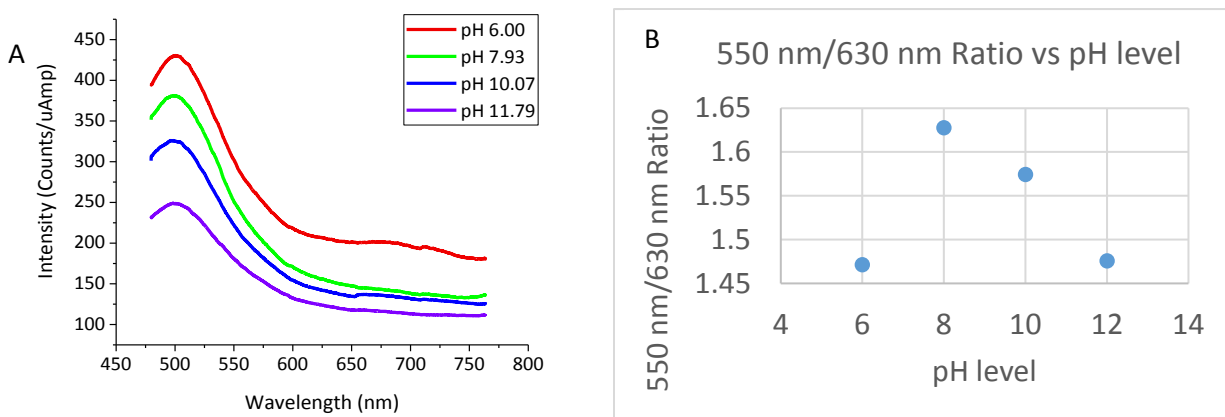
Figure 5 *(a) Fluorescence spectra of GO in aqueous suspension at various biological pH levels.*

(b) Green to red emission intensity ratios with respect to pH level.

In the acidic limit GO emission is centered in red and tails into near-IR, however in the biological pH limit the emission varies significantly between red and green. The variations between emission intensities in green (550 nm) and red (over 630 nm) for acidic to basic pH allow us to envision ratiometric sensing of cancerous environments: we propose utilizing ratios of red to green emission that appear to be different for acidic and regular pH environments (Figure 5) for detection and assessment of different pH. As pH changes from 6 to 8 (Figure 5) the green to red emission ratio decreases by the factor of approximately 1.4. This suggests the potential application of GO as a potential sensor for acidic environments present in cancer tumors occurring as a result of cancer cells excreting more lactic acid[101].

2.2 Graphene Quantum Dots

2.2.1 Synthesis

Graphene quantum dots are synthesized using a microwave-assisted treatment procedure, and is completed using a commercial microwave. A glucosamine solution is placed in a microwave and treated for 40 minutes at a power setting of 450 W. The graphene quantum dots produced using this method are then purified from the smaller-sized via bag dialysis with 500-1000 Da membrane for seven days. A substantial synthesis yield of 15-20% is achieved after purification[85]. Different dopant substances (sulfur thiourea or boron precursors) could be added to the hydrothermal synthesis step to achieve different quantum dot types (N-GQDs, NS-GQDs, and BN-GQDs), which show different emission efficiencies due to doping-related fluorescence quenching or enhancement.

2.2.2 Fluorescence

Graphene quantum dots also exhibit fluorescence peaks in the visible to the NIR regions. GQDs used in this work exhibit two emission features: in the visible and in the near-infrared (Figure 6).
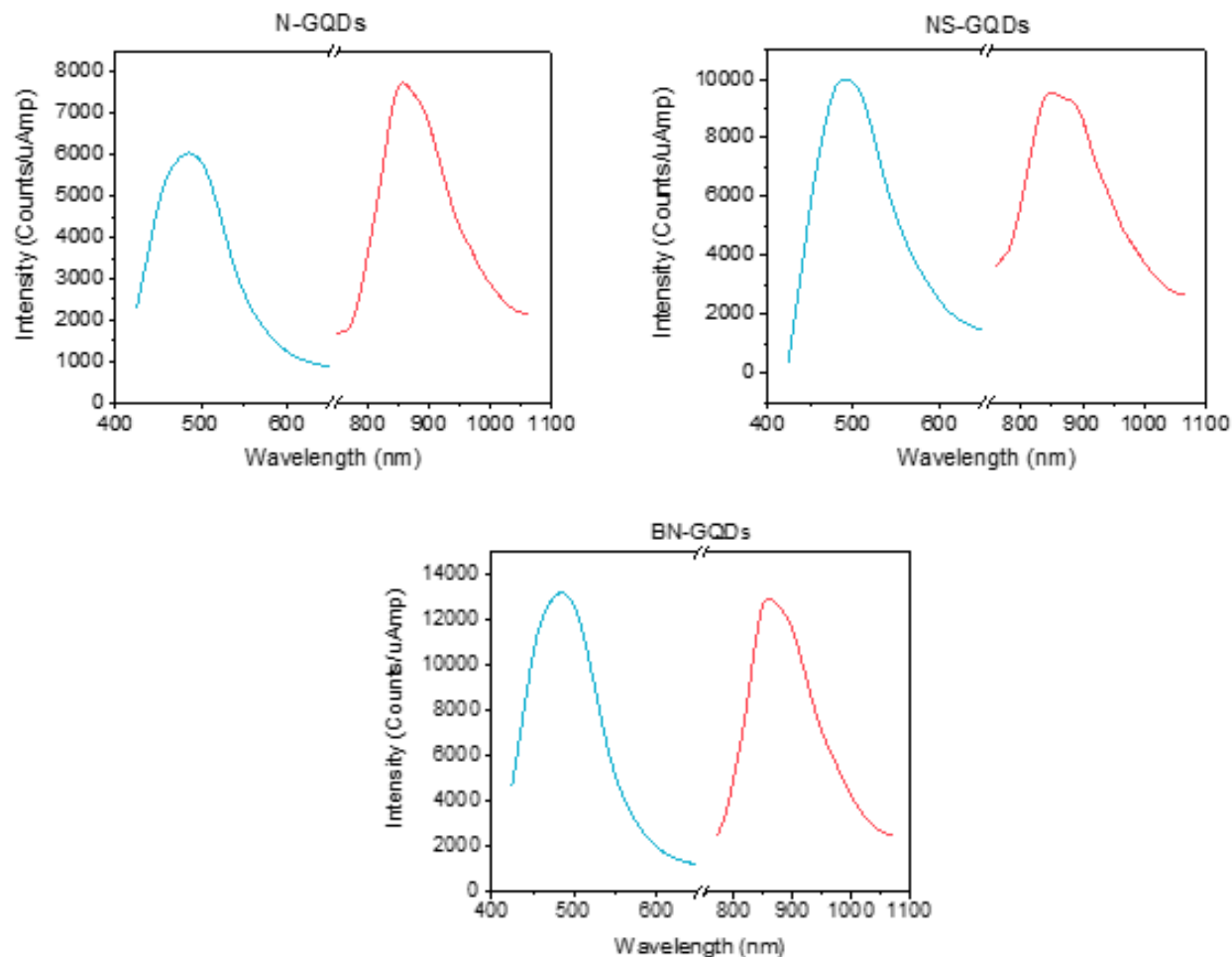
Figure 6 *Emission spectra in visible and NIR for N-GQDs, NS-GQDs, and BN-GQDs*

The emission in the visible range is expected to be confinement-related occurring in the visible due to the small size of quantum dots. This again relates back to the example of a 2D particle in a box, where, as the region becomes confined, the energy levels become quantized. Therefore, the fluorescence emission transitions occur in these confined regions[88]. The emission in the NIR,

however is potentially related to electronic states at the defects or their arrangements[85]. These fluorescence properties possessed by GQDs make them promising materials for potential use in biological applications: NIR imaging allows for a significantly higher penetration depth[83] than that conveyed by conventional visible fluorophores due to less scattering at higher wavelengths, which is beneficial for the further development of this project into animal imaging applications. Thus as fluorophores, GQDs offer the advantage of fluorescing in both the visible, which can be utilized for *in vitro* studies, or in the near-IR for *in vivo* analysis[102]. These fluorescent properties make GQDs a promising platform for image-guided delivery.

2.2.3 Size characterization/Degradation

Graphene quantum dots are an advantageous nano-vehicle due to their size and ability to be doped with other materials, enabling the tuning of their optical properties. As synthesized GQDs show crystallinity and sizes of 3-5 nm derived from TEM images (Figure 7), which suggests easy cell penetration. In order to be compatible for biological studies, ideal imaging/delivery vehicles are desired to be biodegradable to avoid accumulation in the body and increasing residual toxicity associated with that. To verify that graphene quantum dots can be degraded biologically they were imaged in HeLa cell culture over time with TEM. Images of the GQDs at the treatment times of 0-36 hours in HeLa cells demonstrate significant decrease in size and crystallinity resulting in the degradation of the quantum dots over time (Figure 7). At 24 hours, GQD sizes tend to become smaller and they lose their circular shape.
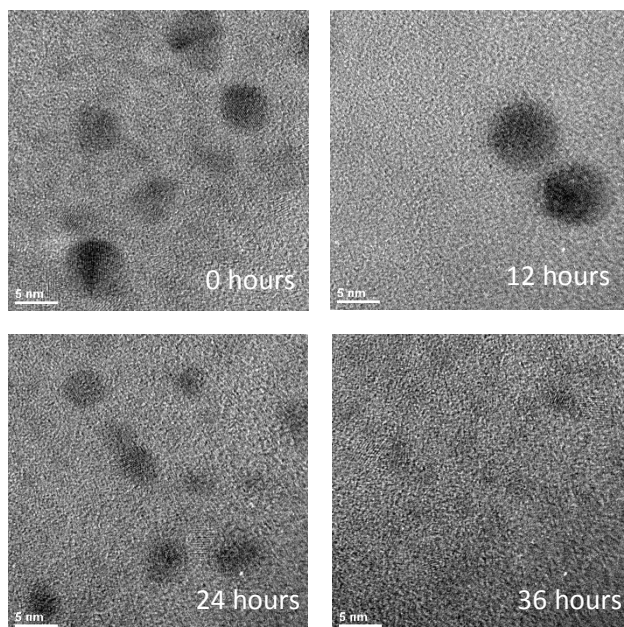
Figure 7 *TEM images of N-GQDs for varying treatment times in cells. Scale bar is 5 μm.*

By 36 hours, the quantum dots appear to be partially - to fully degraded. Currently, we hypothesize that the degrading parts are separated in a form of glucose-based monomers that are further metabolized by the cells. Further experimentation will be performed to verify this hypothesis.

2.2.4 Cytotoxicity

Again, the toxicity was evaluated to verify the validity for the use of graphene quantum dots for *in vitro* and *in vivo* studies and applications. HeLa cells were treated with BN-GQDs, NS-GQDs, and N-GQDs up to maximum concentrations allowed by the synthetic procedure but no significant cytotoxic response was observed for NS-GQDs and N-GQDs. Both NS-GQDs and N-GQDs show over 90% cell viability at the imaging concentrations of 1 mg/mL as indicated by the MTT assay (Figure 8). The apparent increase in cell viability at lower cell doses could be potentially explained that QDs may have partially degraded to glucose feeding the cells and improving their proliferation. NS-GQDs AND N-GQDs concentrations are not expected to limit use in patients due to this low cytotoxic response.
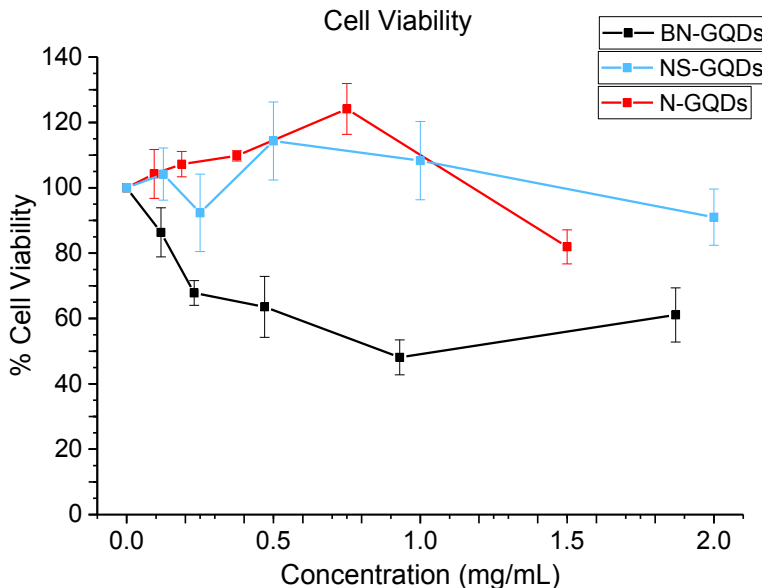
Figure 8 *Cytotoxicity of BN-GQDs (black), NS-GQDs (blue), and N-GQDs (red) in HeLa cells showing percent cell viability with respect to the GQD concentration.*

The absence of significant cytotoxic response of the cells to high concentrations of these quantum dots shows that they have the potential to be used in multiple bio applications. HeLa cells did, however, display a higher cytotoxic response when introduced to the BN-GQDs with below 60% cell viability, thus hindering their future use *in vitro* and *in vivo* at the concentrations above 0.1 mg/mL. The MTT cytotoxicity assay was again conducted using serial dilutions at the testing concentrations ranging from 0 to 2 mg/mL.

2.2.5 pH dependent spectra

For GQDs to also be used as a sensing mechanism, we explored their ability to detect the difference in pH of their environments. Fortunately, their emission exhibit substantial dependence of pH and the most significant variation of their spectra fall within the biological pH range.
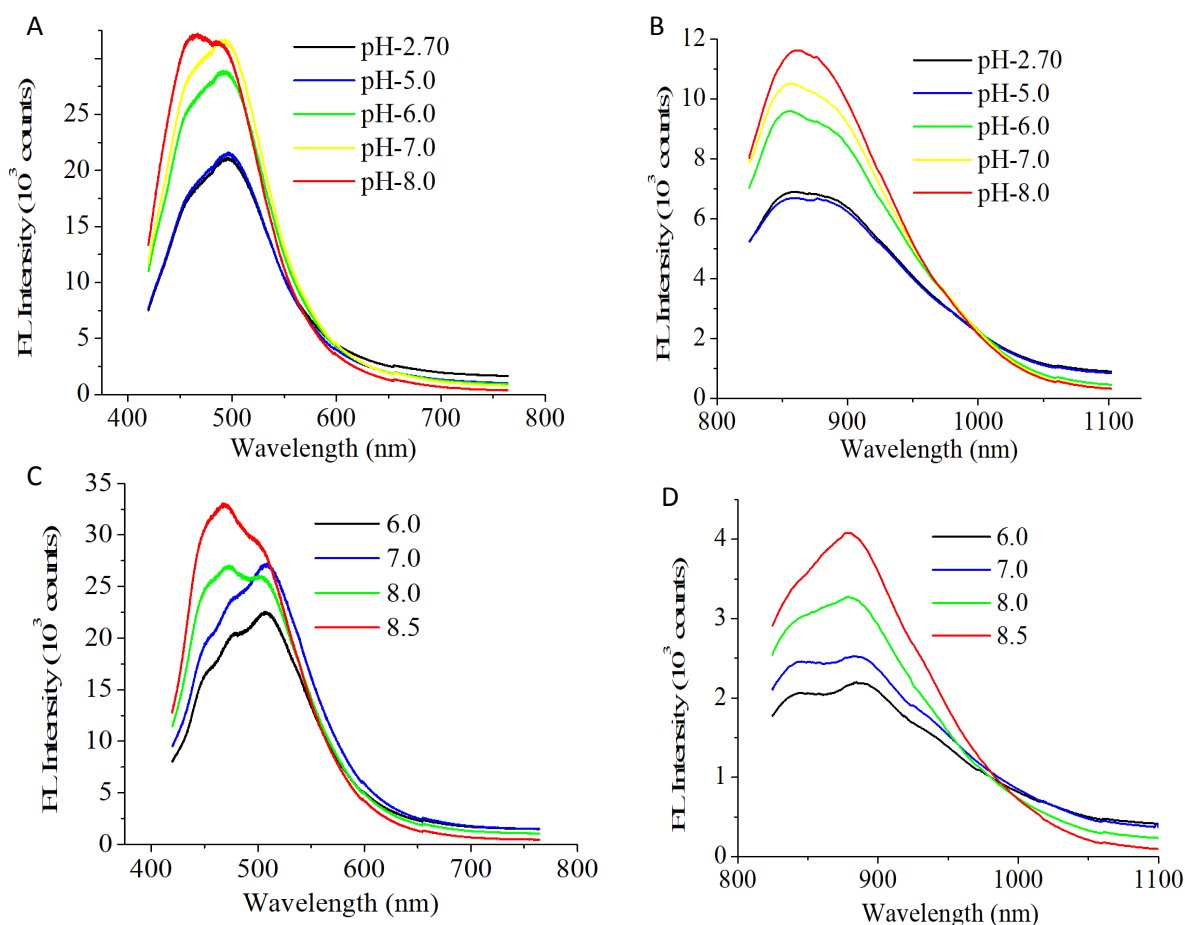
Figure 9 *Fluorescence spectra of N-GQDs at varying pH levels in (a) visible, (b) NIR and NS-GQDs in (c) visible, (d) NIR region. Uncertainty in spectra is below line width; no quenching is observed.*

As can be seen in Figure 9, there are substantial changes in the spectral shape within the spectra between pH 6 and 8. At the basic pH – blue and at the acidic pH – green shoulder of their spectra become more dominant. The emission intensities are changed between green (550 nm) and blue (450 nm) peaks by a factor of approximately 1.7 for N-GQDs and 1.6 for NS-GQDs. Though slight, this effect can allow us to differentiate between low pH and biological pH environments first, spectrally. We hypothesize that the ratio between these two peaks can be used for detection of a cancerous environment, and N-GQDs and NS-GQDs could be used as sensing agents in cancer and healthy cell types. The emission spectra for BN-GQDs shows no shift in the spectra,

potentially, due to the passivation by of some of the functional groups by boron dopants and therefore cannot be used for cancer detection.

CHAPTER- 3
IMAGING CAPABILITIES

3.1 Graphene Oxide

3.1.1 Emission of sample vs. control

Here we test the capabilities of GO as an imaging agent for tracing the delivery pathways of therapeutics delivered by GO platform. As a fluorophore, graphene oxide exhibits fluorescence with a quantum yield of approximately 1%[91], though some report quantum yields of up to 10%[103] in the visible and also near-IR where the biological autofluorescence background is diminished. This makes red/near-IR emissive GO used in the present study an advantageous agent for biological imaging. In this work we optimize and test GO for that application: we used 480 nm excitation, while detecting GO emission in red (630 nm) to achieve imaging of cancer cell environments. Excitation and emission wavelength ranges were selected on the basis of the spectral analysis of GO emission features and its excitation spectra[91].

Figure 10 *Fluorescence microscopy. (a) HeLa cells transfected with GO (b)Fluorescence image of non-treatment control HeLa cells (c) Overlay of fluorescence and bright field image for non-treatment control HeLa cells.*

In order to account for autofluorescence from cells, imaging settings (integration time and gain) were chosen such that there was zero autofluorescence observed from a number of cells in control samples (Figure 10b). The ability of GO to internalize and provide fluorescence imaging in cancer cells was verified by introducing GO suspension into HeLa cell culture for 1 hr. GO-treated HeLa cells were washed prior to imaging to remove any extracellular GO adhering to the cell membrane so that the GO we see in images could be situated only within the cells. Microscopy images indicate substantial 630 nm emission from nanoscale GO flakes inside the cells (Figure 10a). Individual GO flake structures are not resolved, as internalized flake dimensions are expected to be under 300 nm[104,105]. We have specifically decreased the integration times and lamp intensities so that the autofluorescence from the cells would be below the noise level (Figure 10b, 10c). Thus, the GO emission that is observable with these settings is significantly above the autofluorescence. At the same imaging conditions, non-treated cells show no observable emission (Figure 10b, 10c).

3.1.2 Internalization

GO-based imaging in HeLa cells provides a unique capability not only to track GO and potentially its payload but additionally to assess the internalization and excretion of GO from the cells. Considering that no photobleaching was recorded for individual GO flakes over time, the increase of GO emission in cells is attributed to internalization, while decrease - to excretion. Since we expect more effective internalization with smaller nanoparticle size, alteration of GO size by ultrasonic treatment allows for more efficient internalization. To achieve optimal internalization and imaging conditions, we explored the influence of transfection time and the size of GO flakes on the internalization efficiency.

Emission from GO formulations processed by different ultrasonic treatment routines was observed in HeLa cells at 1, 3 and 12 hours post transfection (Figure 11). GO externally attached to cell membrane was removed by two consecutive washing procedures leaving mainly the emission from internalized flakes. The matrix of images for different ultrasonic treatments versus transfection times shows the highest emission processed by 30 and 50 min of ultrasonic treatment (corresponding flake sizes of 202 nm and 190 nm) at 3W power at the transfection times of 1 to 3h.

As predicted, the aggregation of the 60 min treated GO leads to low intracellular GO emission (Figure 11) thus setting a limit of 190 nm for effective flake sizes used in this work. The general trend in this study showed less emission at 12 hours for smaller flake sizes, which indicated potential excretion of graphene oxide from the cells. Knowing the optimal flake size (average long axis dimension of 202 nm corresponding to 30 min ultrasonic treatment time), we used it to determine the optimal internalization/excretion time frame for GO as a therapeutic carrier over time periods of 30 min to 24 hr. ImageJ software was used for image analysis including calculations of background-subtracted emission per unit area and per biological cell. Background intensity per unit area was calculated by taking an average of the mean gray value of the background and multiplying it by the area of each measured region. Corrected total cell fluorescence (CTCF) was determined by taking the integrated intensity over the whole cell and subtracting out the average background intensity determined from three different background intensity measurements for each image. Error estimates were made by calculating the standard deviation and dividing by the square root of the number of analyzed images. This allows to assess that the normalized fluorescence intensity per unit area is consistently within a small range of values, validating the hypothesized trends.
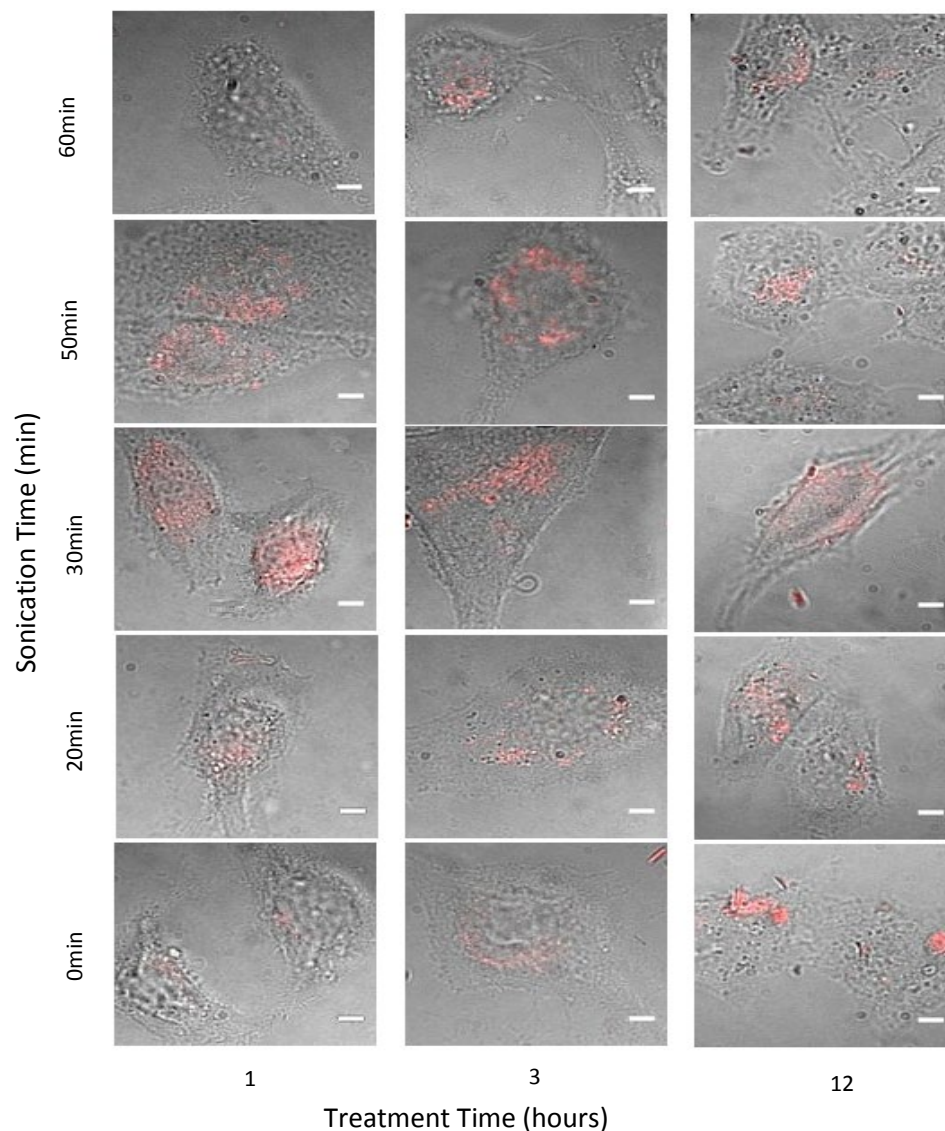
Figure 11 *Image matrix of GO emission in HeLa cells with varying ultrasonic treatment time (vertical) vs. transfection time (horizontal). Scale bar length is 5μm.*

As indicated by the plot of integrated fluorescence intensity per cell (Figure 12), optimal internalization occurs at 1 hr post transfection with the following excretion of GO from the cells down to 30% in 24 hrs. Such rapid internalization with the evidence of further excretion is beneficial for drug transport: quick and efficient delivery of the drug is desirable, while the clearance of the platform from the cells allows to avoid cytotoxicity and cell damage associated with accumulation of the large amounts of nanomaterials.
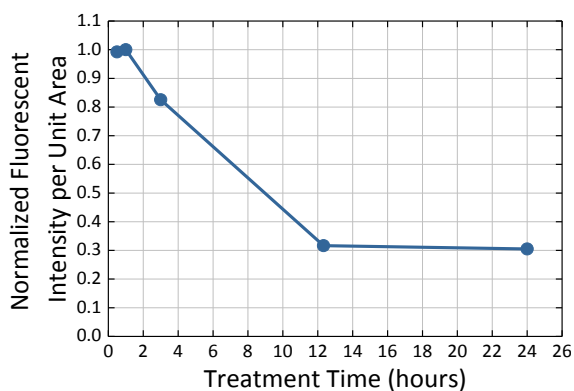
Figure 12 *Intensity per unit area of GO emission from HeLa cells depending on the treatment time. Error bars are within the size of the points.*

Colocalization studies allow us to infer the function and/or location of a molecule through its association with certain parts of a cell[106]. These studies are more beneficial than just taking a fluorescent image as they allow to analyze the distribution of particle in comparison to known, labelled parts of the cell itself. Lysotracker green labels the lysosomes within a cell, while DAPI labels the nucleus. Overlay images allow us to determine in which cell compartment graphene oxide localizes after the delivery, which helps understanding the entrance pathways used by the nanomaterial *in vitro*. DAPI and lysotracker green co-staining show in Figure 13b that GO emission does not significantly co-localize with cell nuclei. Only few such sections are seen in the 'purple' (Figure 13 a, b) on the overlay image. However, in a number of cells GO appears to co-localize with lysosomes stained by lysotracker green, suggesting endocytosis as one of the pathways of cellular entry (Figures 13a, c) and initial internalization of GO flakes within the lysosomes. These regions are observed as orange in Figure 13 (a and c) overlays, indicating the overlap of the green lysosome stain and the red GO emission. Due to a high amount of charged functional groups we expect GO to destabilize ionic pressure in endosomes facilitating further escape.
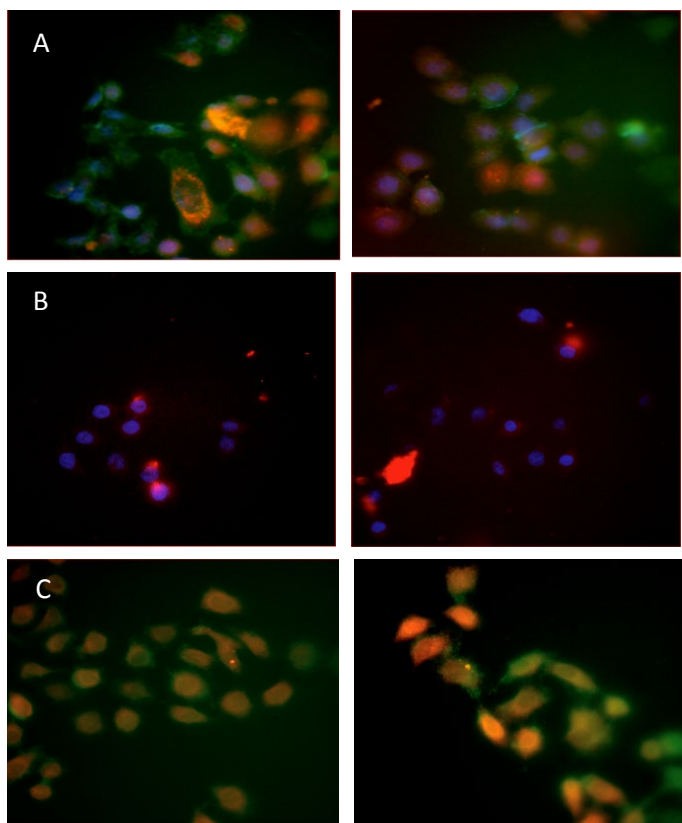
Figure 13 *A) Colocalization images of GO emission (red) with DAPI (blue) and Lysotracker Green (green) staining within HeLa cells. B) Fluorescence imaging: GO + DAPI staining of HeLa cells. C) Fluorescence imaging: GO + Lysotracker green staining of HeLa cells.*

This colocalization also adds to the proof of cellular internalization suggesting the potential of GO as an imaging and therapeutic delivery agent.

3.2 Graphene Quantum Dots

3.2.1 Emission of sample vs. control

Similar to the evaluation of GO, we then tested the capabilities of GQDs as imaging agents for tracing the delivery pathways of therapeutics transported by GQD platforms. In this work we optimize and test N-GQDs, NS-GQDs, and BN-GQDs for that application: imaging both in the visible and near-infrared. Internalization studies were conveyed *in vitro*, thus visible imaging was utilized with 475 nm excitation, while detecting GQD emission at 535 nm to achieve imaging of

cancer cell environments. As the visible GQD emission usually showed slightly higher intensity than that in NIR, we conveniently used that for cell imaging, where as opposed to animal models deep tissue penetration of NIR emission is not required. Excitation and emission wavelength ranges were selected on the basis of the spectral analysis of each of the GQD emission features and excitation spectra (Figure 9). Integration time, gain, and lamp intensity were adjusted such that the signal from the quantum dots was brightest with the lowest autofluorescence signal from the HeLa cells (Figure 14). This allows us to hypothesize that the emission signal detected is coming almost exclusively from the graphene quantum dots. Additionally the cells were washed prior to imaging thus no extracellular GQD emission is expected to interfere with cell imaging. Each graphene quantum dot type was introduced to HeLa cells in an aqueous solution and imaged after 1 hour transfection time.
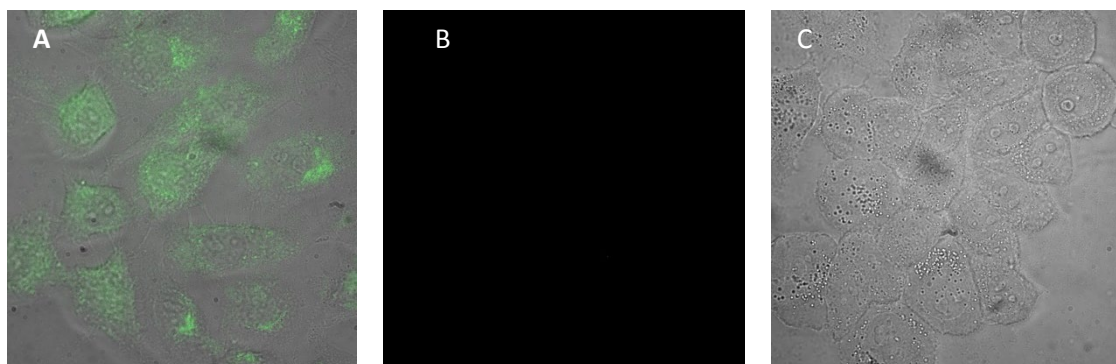
Figure 14 *Fluorescence microscopy. (a) HeLa cells transfected with GQDs (b)Fluorescence image of non-treatment control HeLa cells (c) Overlay of fluorescence and bright field image for non-treatment control HeLa cells.*

As can be seen in Figure 14, GQD emission significantly well above the autofluorescence level of the cells, while non-treated cells show no observable emission at the conditions chosen in this experiment. This is expected as the quantum dots synthesized in our works have generally substantially higher quantum yields than GO.

Another exciting application of the quantum dots studied in this work is their potential use for multicolor imaging. These nanomaterials have stable fluorescence that does not show detectable fluctuation with prolonged irradiation that has features in the visible and the near-IR, allowing for potential *in vivo* studies, as the near-IR yields deeper penetration into biological tissues. If successful, this would allow for non-invasive optical imaging of the therapeutic pathways simultaneously with drug delivery in animal. Each quantum dot type was imaged at a variety of excitation and emission wavelengths, and shows emission in blue (450 nm), green (535 nm), and NIR (750 nm) (Figure 15). A capability of imaging across different spectral regions makes quantum dots even more desirable for potential applications utilizing image-guided therapy: they become more versatile imaging agents that, depending on the need, can be imaged at different wavelengths *in vitro* and also in the near-infrared *in vivo*.

N-GQDs
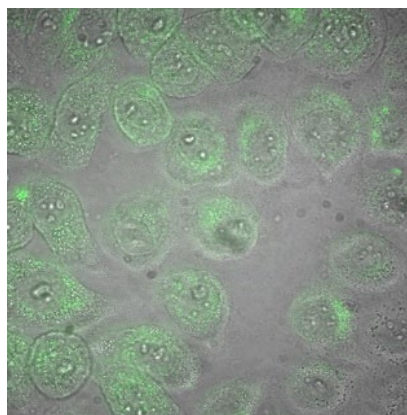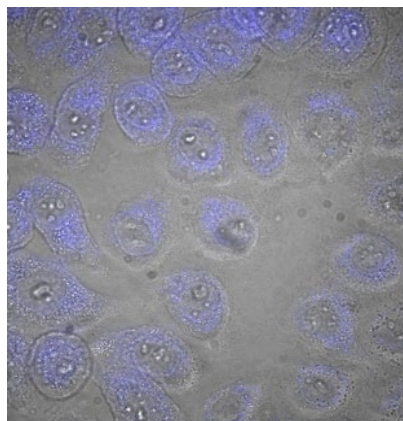
NS-GQDs
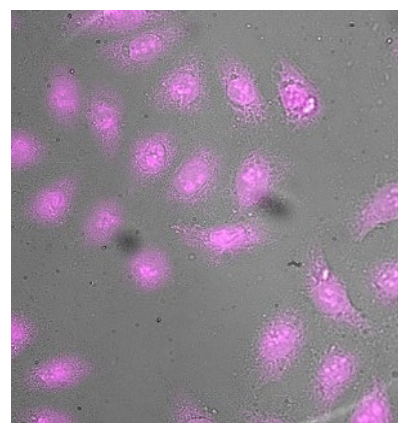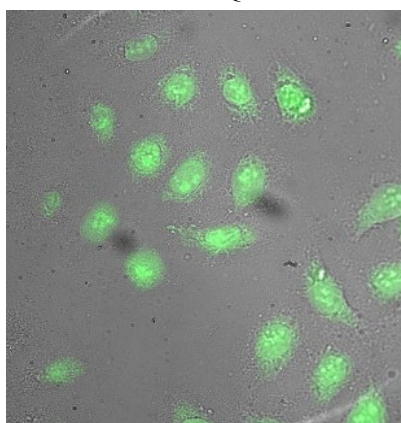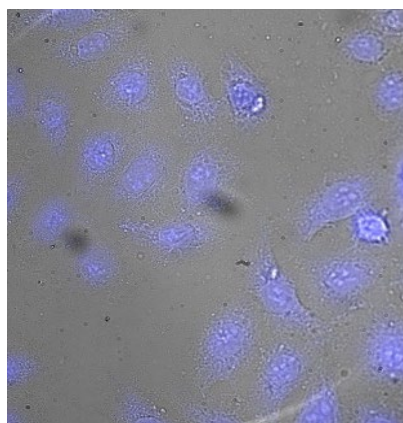
BN-GQDs
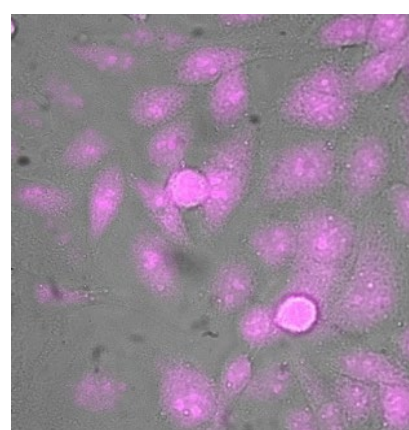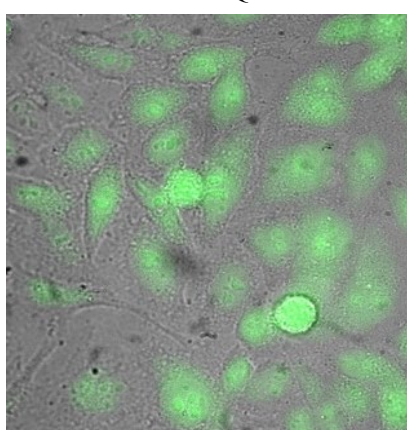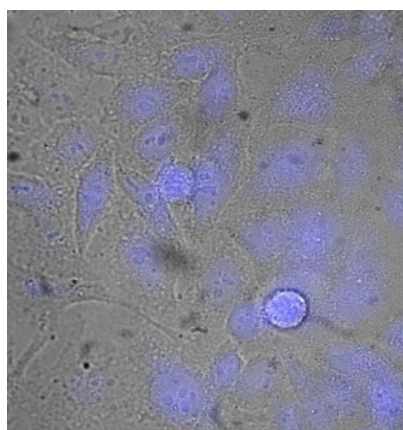
Exc: 375 nm; Em: 450 nm   Exc: 475 nm; Em: 535 nm   Exc: 650 nm; Em: 750 nm

Figure 15 *Multicolor imaging of N-GQDs, NS-GQDs, and BN-GQDs in blue, green, and near-IR.*

3.2.2 Internalization

An internalization study for GQDs is critical for evaluating the treatment time for the different types of quantum dots. Here, the maximum intensity is assumed to be the maximum internalization point, as the HeLa cells underwent a washing step prior to imaging, to remove any extracellular material including quantum dots. This left only the GQDs that have internalized into HeLa cells. Each type of quantum dots was imaged *in vitro*, allowing us to determine the time-point for maximum internalization. In order to assess the internalization, we recorded the fluorescence intensity per unit cell area for over 100 cells with backgrounds subtracted in the ImageJ software. Since all GQDs outside the cells were removed, that emission signal was deemed to be proportional to the amount of GQDs internalized into cells and thus was plotted with respect to time to assess the most efficient internalization time frame. Internalization plots for N-GQDs, NS-GQDs, and BN-GQDs shown in Figure 16 indicate that the 12 hour treatment point provided the largest fluorescence intensity for all quantum dot types. Similar internalization is expected as the GQDs tested in this work had similar structures and only varied in doping types and levels affecting electronic properties and toxicity.
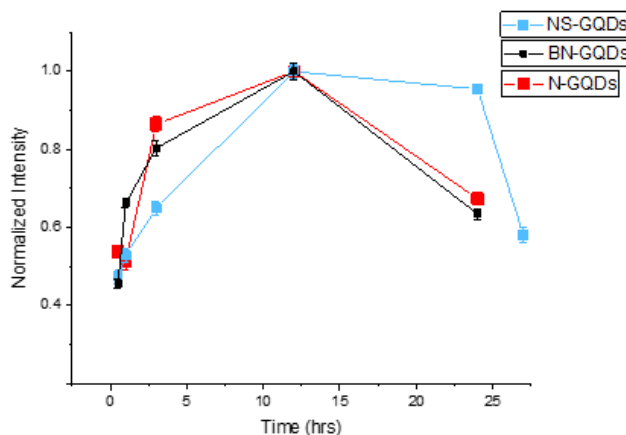
Figure 16 *Cell internalization/excretion plots for N-GQDs (red), NS-GQDs (blue), and BN-GQDs (black). Error bars for some points are within their size.*

The general trend in this study showed less emission at 24 hours for each quantum dot type, which indicated potential excretion of GQDs from the cells. This is important, as future *in vivo* studies would require the excretion of the nanovehicle to minimize its toxicity to cells and cell deformation through over-accumulation observed with multiple other nanomaterials[107]. The internalization and excretion trend can also be evidently seen in the representative images when comparing the emission intensity at different treatment times (Figure 17).
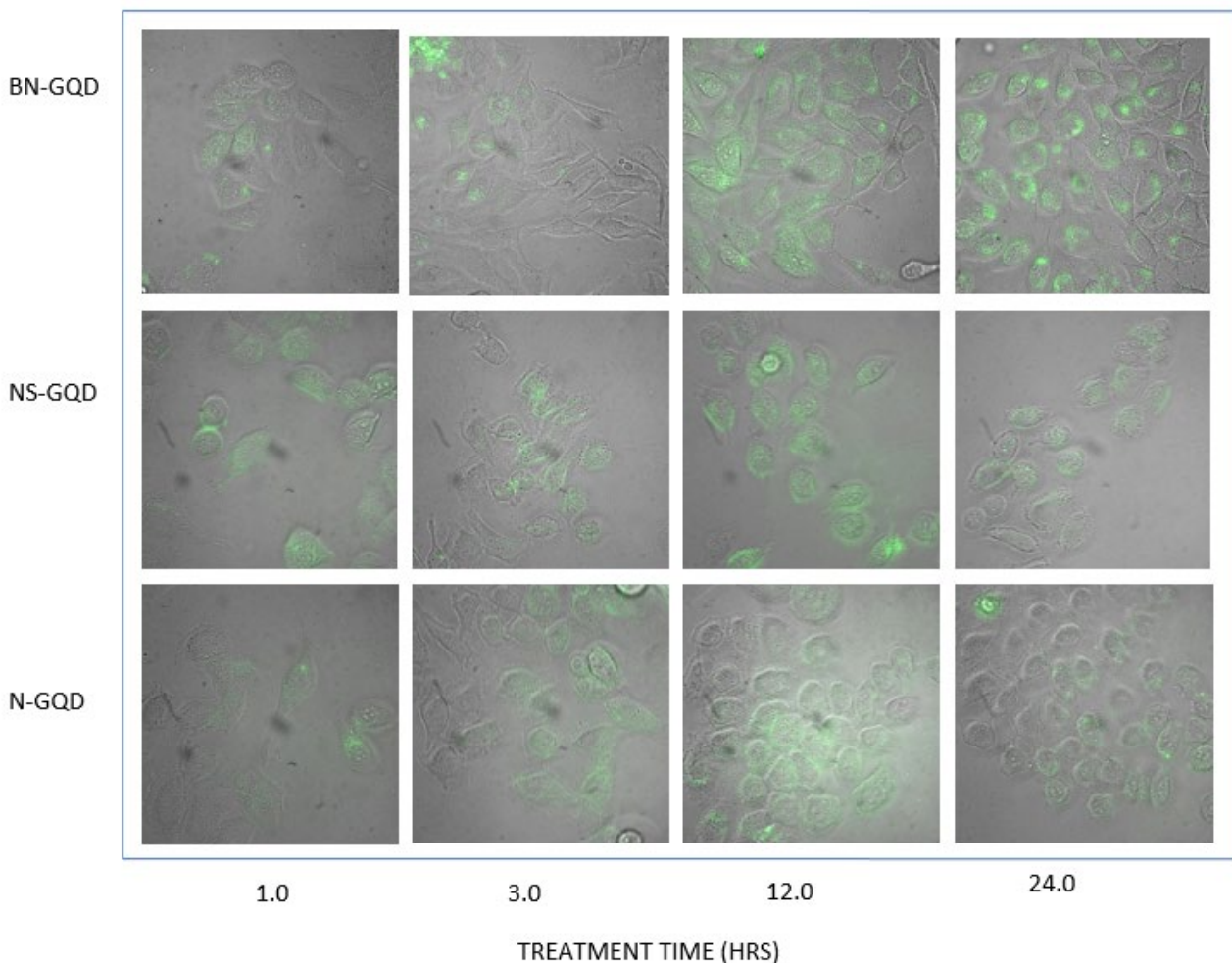
Figure 17 Image matrix showing quantum dot type vs treatment time points. Excitation 475 nm emission 535 nm.

It is clear that the emission signal in cells is increasing between the 1 and 3 hour transfection images with the peak at 12 hours and decrease post 24 hours (except for BN-GQDs that do take somewhat longer to excrete). As more cells are illuminated with green emission at 12 h time point, we expect that the graphene quantum dots are at maximum internalization within the cell. Again, the autofluorescence emission from these cells is kept below the noise levels.

CHAPTER- 4

SENSING CAPABILITIES

4.1 Graphene Oxide

4.1.1 Individual sensing capabilities
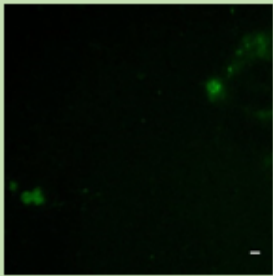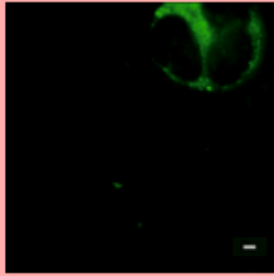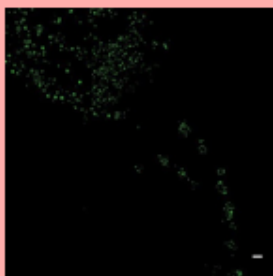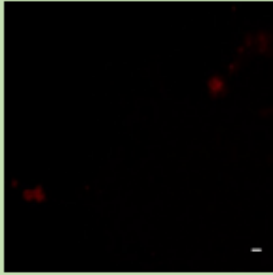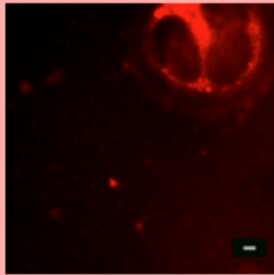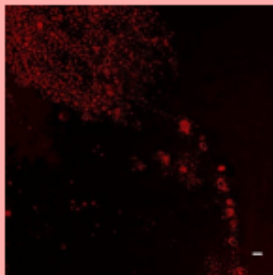
In addition to imaging and successful internalization, the optimized GO flakes show the capacity of pH-based detection of cancerous environments. Since cancer cells excrete lactic acid[101], tumor regions maintain acidic environments at approximately pH 6 at which GO shows a markedly different emission signature than at a regular pH of 7-8 [108, 109, 110]. According to spectral dependence of GO emission on pH of the environment, we propose using it as a microscopic pH sensor and test GO flakes for detection of pH at the microenvironments. At the single flake level (Figure 18) we observe brighter emission in red (630 nm) than green (550 nm) for the more acidic (pH 6) environments, and a quenched red emission for more basic (pH 8) environments. Quantitatively this results in average green to red emission intensity ratios of 0.548 and 0.777 calculated per unit area for pH 6 and 8, respectively integrated for over 400 individual flakes. The difference in emission on the single flake level leads us to assume that such sensing will be possible within cellular environments.
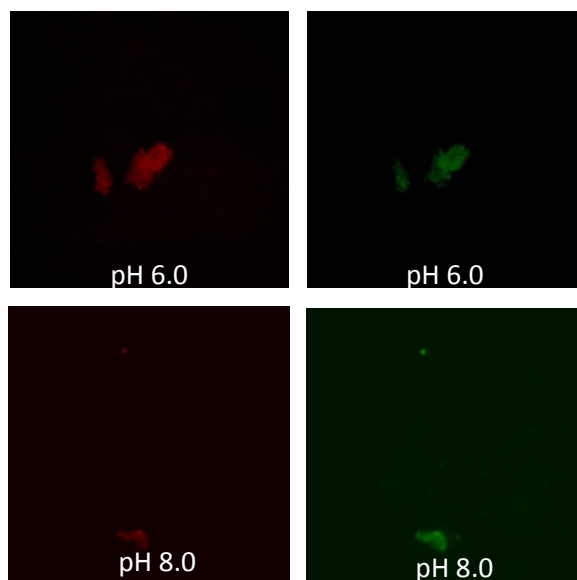
Figure 18 *Fluorescence of individual GO flakes at pH 6 vs 8 in red (630 nm) versus green (550 nm) with 480 nm excitation.*

4.1.2 Sensing capabilities *in vitro*

In order to verify the *in vitro* sensing capabilities, we introduced GO suspension subjected to 30-minute ultrasonic processing (optimal for internalization) to two cancer and one healthy cell lines (HeLa, MCF7, and HEK-293) without washing so that the extracellular GO will be retained. That way we aim to detect the pH of both intracellular and extracellular environments using the emission signal. The statistics of GO emission in green (550 nm) and red (630 nm) for the pH analysis of cancer versus healthy cells was obtained by performing measurements on over 100 cells for each excitation wavelength. The images taken were of the same cells, allowing for the analysis of the exact same objects in both red and green.

550/630 nm Intensity Ratios			
	HEK-293	HELA	MCF-7
INTRACELLULAR	0.93 ± 0.04	0.91 ± 0.03	0.91 ± 0.01
EXTRACELLULAR	0.82 ± 0.04	0.62 ± 0.03	0.72 ± 0.01
Green			
Red			

Table 1 *Comparison of intracellular vs. extracellular green/red intensity ratios across healthy (HEK-293) versus cancer (HeLa and MCF-7) cell lines, and images demonstrating fluorescence differences for extracellular environments: emission in red is brighter for cancer cells. Scale bar= 5μm.*

Again, CTCF was determined by highlighting the fluorescent regions in red and green and subtracting out the average background intensity in the area equal to that of the highlighted regions. The CTCF for red and green GO emission were then compared for intracellular and extracellular data sets, allowing for the quantification of the green to red emission ratios. As the pH of the intracellular environment was not expected to vary greatly due to the internal cell buffering
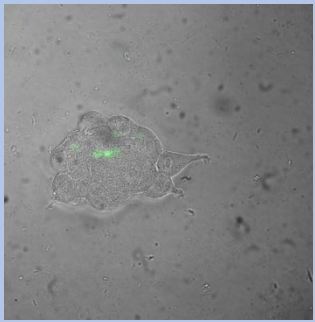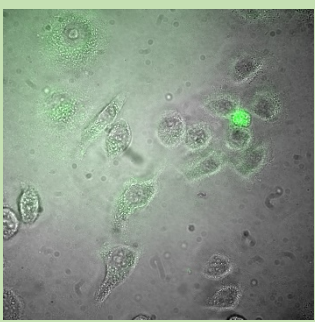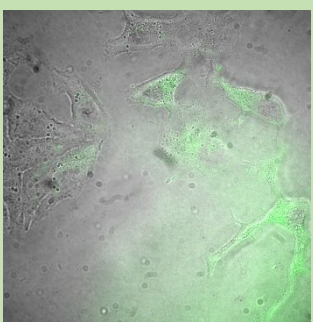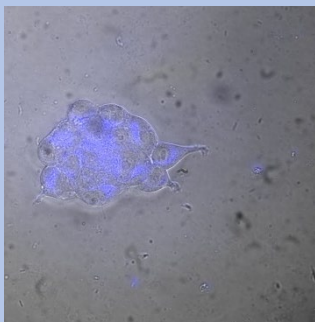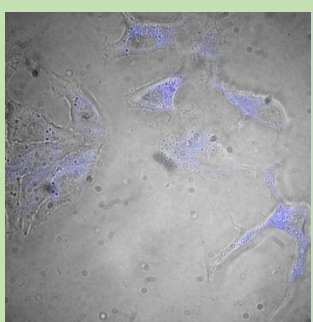
capacity[111,112], we saw very little differences in green/red ratios of intensity per unit area for intracellular GO emission in either cell type (Table 1). This effect is dictated by the pH buffering by cell proteins and phosphate buffers in intracellular compartments restricting pH within a narrow range of approximately 7.1-7.2[112,113]. Statistical analysis of scattered GO flakes located in the extracellular environments, however, show that green/red ratios of intensity per unit area are greater for healthy rather than cancer cells (Table 1). This relative difference of 13-25% also potentially affected by pH buffering of cell media, provides a significant variation to be used for the detection of cancerous environments, given only 2% difference between such ratios intracellularly and the large sampling size of over 500 flakes. This suggests a promising potential of GO as a nanoscale local sensor of cancerous environments either *in vitro*, *ex vivo* or intravitally using techniques developed for protein sensing[114] or for determination of tumor borders in surgical procedures[115]. pH-sensing capacity of GO can be also utilized for applications other than cancer such as detection of microscopic pH changes in media, drug screenings, and assessment of cellular processes [116, 117].

4.2 Graphene Quantum Dots

4.2.1 Sensing capabilities *in vitro*

pH-sensing is important for these platforms as this would add to the modalities in which such formulations could be used, such as cancer detection[118], sensors to be used for glucose detection[119] or nucleic acid probing[120], and the development of multifunctional imaging, sensing and delivery platforms. Many nanomaterials fail to offer the efficiency of simultaneous imaging, delivery, and sensing[121,122]. This capability would add to the remarkable properties of GQDs, making them a fully multifunctional agent. To verify the sensing capabilities of the N-GQDs and NS-GQDs, we introduced suspension of each quantum dot type to two cancer and one healthy cell lines (HeLa, MCF7, and HEK-293). Again, cells were imaged without a washing step so that the
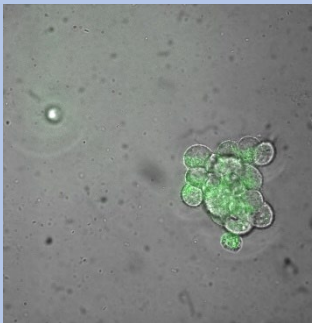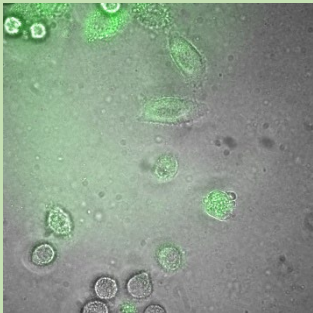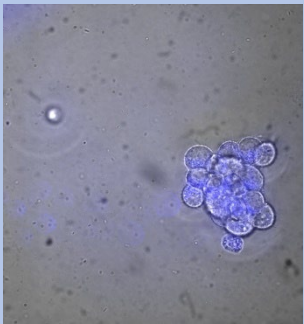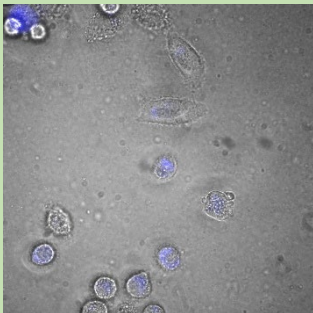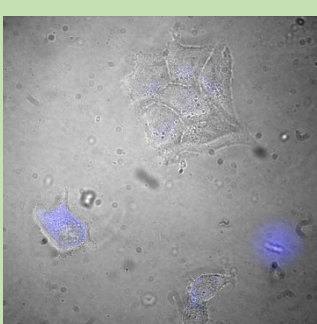
extracellular quantum dots will remain: the pH sensing of extracellular environments could be an important marker of high extracellularly excited lactic acid levels. Thus here, similarly to GO, we aim to detect the pH of both intracellular and extracellular environments using the emission signal from quantum dots.

535/450 nm Intensity Ratios Across Cell Lines N-GQDs			
	HEK-293	HELA	MCF-7
INTRACELLULAR	1.73 ± 0.49	2.56 ± 0.05	2.27 ± 0.63
EXTRACELLULAR	1.22 ± 0.01	8.27 ± 0.05	8.38 ± 0.63
Green			
Blue			

Table 2 *Comparison of N-GQDs intracellular vs. extracellular green/blue intensity ratios across healthy (HEK-293) versus cancer (HeLa and MCF-7) cell lines, and images demonstrating fluorescence differences for extracellular environments: emission in green is brighter for cancer cells. Scale bar= 5μm.*

The statistics of GQD emission in green (550 nm) and blue (450 nm) were compared for images taken of the same cells for over 100 cells at each excitation and emission wavelength. The CTCF was determined by accounting for the average background intensity in each sample. These corrected values were then used for the ratios found in Table 2 and 3. Table 2 describing the emission ratios and providing visuals for N-GQD emission at a particular wavelength in cancer verses healthy cells shows that there is a minor trend amongst the intracellular ratios. This is due to the fact that pH buffering by cell proteins and phosphate buffers maintain the pH within a narrow biological range [112,113]. Extracellular ratios, however, vary significantly between healthy (HEK-293) and cancer (HeLa, MCF-7) cell lines. Green to blue ratios are larger for cancer cell type extracellular environments, indicating more emission in green (acidic pH) than blue (regular pH), whereas the opposite trend is true for the healthy cell type samples. This distinction between cancer and healthy extracellular environments suggests that GQDs can be used as sensing agents *in vitro*. The results found for the N-GQDs were comparable to those found in the NS-GQDs (Table 3): the intracellular ratios again offer only a mild change between cancer and healthy cell types, whereas extracellular green/blue emission ratios offer significant differentiation between the cancer and healthy environments. This is confirmed visually by the images of GQD emission in green and blue in cancer versus healthy cell types (Tables 2, 3). The emission of BN-GQDs does not indicate pH-dependence spectrally and was not analyzed *in vitro* for pH-based cancer detection. The ratios observed in this work differ from those expected from the variation of GQD spectral signatures with pH. Such a dissimilarity can be explained by the effect of biological redox environment not present in aqueous suspensions on protonation and deprotonation of functional groups, and additionally by integration of the emission intensity over the spectral range permitted by the microscopy filters. GQDs in biological cell experiments are also generally imaged near the

cells providing sensing of pH microenvironments in the vicinity of the centers of lactic acid excretion where the immediate concentrations of excreted lactic acid could be higher.

535/450 nm Intensity Ratios Across Cell Lines NS-GQDs			
	HEK-293	HELA	MCF-7
INTRACELLULAR	1.09 ± 0.01	2.18 ± 0.35	1.73 ± 0.09
EXTRACELLULAR	1.50 ± 0.01	4.96 ± 0.35	3.57 ± 0.09
Green			
Blue			

Table 3 *Comparison of NS-GQDs intracellular vs. extracellular green/blue intensity ratios across healthy (HEK-293) versus cancer (HeLa and MCF-7) cell lines, and images demonstrating fluorescence differences for extracellular environments: emission in green is brighter for cancer cells. Scale bar= 5μm.*

Nevertheless *in vitro* work reveals a more efficient cancer sensing that provides a promise of using of GQDs as nanoscale pH sensors *in vitro* and due to the pH-dependence of NIR emission also indicates the potential for GQDs to be applied as sensors of cancerous environments *in vivo* for future works.

In addition to cancer detection, graphene quantum dot imaging and sensing can be utilized for a variety of applications, including electrochemical biosensors[123,124], photostable bioimaging[125], and optoelectronic devices[85]. Electrochemical sensors utilize GQD-modified electrodes, and have demonstrated high selectivity and sensitivity[123]. Imaging and sensing capabilities of GQDs can be beneficial for bioimaging insofar as they offer higher photostability and a higher quantum yield (up to 62%)[85] as opposed to many other nanomaterials[125]. GQDs have also been utilized for optoelectronic devices such as solar cells[126] and LEDs[85].

There are also a multitude of applications utilizing the imaging, sensing, and delivery capabilities of graphene quantum dots that have not yet been explored and we envision those as potential future GQD research areas. For example, NIR fluorescence of GQDs could be used for imaging different diseases of the eye such as glaucoma which causes damage to the optical nerve due to eye pressure[127], CMV retinitis which attacks light sensing cells in the eye[128], or other prominent ocular diseases such as age-related macular degradation[129]. Additionally, pH sensing of GQDs could be used for patients who suffer from chronic acidosis, entailing accumulation of acidic compounds in the blood, or other alkaline related diseases. We envision GQDs to be potentially be used as drug delivery, sensing, and/or imaging moieties for a number of these diseases. We also hypothesize the use of GQDs for therapeutic delivery/imaging in the brain for brain cancer/tumor treatment as they possess a very small size resulting in a possibility for penetration of the blood brain barrier[130]. If able to penetrate into brain tissue, for example, GQDs

could aid the treatment of brain tumors, as well as other diseases of the central nervous system[131]. Likewise, due to the fact that NIR fluorescence can penetrate through the layers of biological tissue, including parts of the skull[132], quantum dots offer optical advantages for image-guided treatment at different parts of the body. It could therefore be possible to image drug delivery to the eye and/or the brain, for example, more simply and effectively than with for visible fluorophores that are limited by the penetration depth. For example, NIR fluorescence imaging would allow nearly 360-degree imaging if drugs delivered to the back of the eye in animal studies. Therefore, we envision that with the proper experimental investigation GQDs could offer simultaneous imaging, sensing, and treatment for diseases even beyond the scope of cancer therapies.

CHAPTER- 5
CONCLUSIONS

5.1 Conclusions

In this work we have tested both GQD and GO novel nanoscale platforms for imaging internalization, biocompatibility and cancer sensing. Based on our findings we suggest that graphene oxide can be used as a multifunctional imaging, delivery, and cancer-sensing agent. GO used here exhibits low to no toxicity at the imaging doses, which opens a possibility for further animal studies with this material. The most efficient cellular internalization of GO occurs at 1 hour post transfection and at the smaller flake sizes of ~200 nm that can be simply achieved by 30-minute ultrasonic treatment. In this form, GO can be used as a delivery agent that internalizes quickly and with 70% excretion after 24 hours. pH-sensitive GO emission not only allows to detect its presence in biological cells, but also provides the means to assess the microscopic pH of the cellular environments. In this work, GO shows efficient discrimination of acidic extracellular cancerous environments of HeLa and MCF-7 cells as versus healthy HEK-293 cells with no significant differentiation between their intracellular environments. This outlines a promising potential of GO as a new candidate for the delivery of drug or gene therapeutics, biological imaging via its intrinsic fluorescence in red/near-IR and detection of cancerous environments *in vitro, ex vivo* or intravitally. GO offers a fully multifunctional affordable in mass production alternative to existing nanocarriers without the need of attaching additional imaging and sensing moieties that contribute to the toxic profile of the formulation. Additionally, its modifiable platform allows for further variation of GO flake sizes, functional group types and degrees of oxidation allowing to tailor this multifunctional imaging/sensing platform to a variety of applications including

assessment of enzymatic reactions, detection of glucose or DNA, and microscopic optical pH sensing for multi-analyte monitoring.

Here we also develop and test a novel even more advantageous nanomaterial: graphene quantum dots. GQDs utilized in this work have for the first time been developed in our lab to provide unique capabilities not present in other current GQD platforms. We also propose graphene quantum dots as imaging, sensing a delivery agents for cancer therapeutics. However GQDs have superior properties of smaller size, no cytotoxicity, ease in preparation and apparent biodegradability. Toxicity analyses show that within the imaging concentrations used throughout the study, N-GQDs and NS-GQDs are essentially harmless to the cells, while BN-GQDs offer some cytotoxic response and should be restricted to lower concentrations of ~0.1mg/mL. Each quantum dot type is approximately 3-5 nm in size, therefore making them easily internalized by the cells, with their maximum internalization occurring at 12 hours. This is verified both visually and analytically, indicating that the GQDs are also excreted within 24 hours, making them suitable for drug delivery as they are not expected to accumulate in cells for an indefinite time as many current delivery vehicles do. Additionally, GQDs studied here are biodegradable with over 36h degradation period allowing time for drug release and at the same time making them safe to use in living organisms as they are not expected to accumulate and are hypothesized to degrade in glucose-based monomers. N-GQDs, NS-GQDs, and BN-GQDS all exhibit fluorescent emission that peaks both in the visible to the near-IR, suggesting their imaging capabilities are superior to other nanomaterials used in biomedical applications only exhibiting visible fluorescence. These GQDs can be used for multicolor imaging, indicating the possibility of imaging in cells via visible fluorescence and in tissues via NIR emission. This fluorescence signal is also pH-dependent, allowing the GQDs to detect a difference between cancerous (HeLa and MCF-7 cells) and healthy

(HEK-293 cells) environments. This study suggests that GQDs have a potential to facilitate a novel approach to a critical biomedical need of imaging *in vitro* and *in vivo*, sensing, and therapeutic delivery. GQDs are affordable, easy to produce, and are fully multifunctional agents possessing the properties which could help revolutionize cancer treatments currently available.

5.2 Questions Answered

i.   Can these nanomaterials be used for biomedical applications?

Both graphene oxide and graphene quantum dots have shown that they can be used for biomedical applications. The size of GO can be altered such that the flakes can be internalized by cells more efficiently without altering the optical properties of the flakes themselves. The GO flakes are non-toxic at the imaging concentrations used in this work, allowing them to be potentially utilized in biological drug/gene delivery studies. . Properties of graphene quantum dots also suggest their successful use in biomedical applications. GQDs are very small (3-5 nm) allowing for effective cellular internalization, and are non-toxic at high concentrations of over 1 mg/mL. Additionally, GQDs show degradation in cell culture after 36h which is beneficial as they are not expected to accumulate in the body for a long time constantly adding to the toxicity profile. This complements the biocompatibility of GQDs suggesting that they can be effectively used for biomedical applications. GQDs can be also scalably produced via green synthetic methods at low cost, which is uncommon for modern drug delivery and imaging agents.

ii.   Can they be used for imaging and delivery?

Graphene oxide can be imaged in the visible and graphene quantum dots – in both visible and near-IR with emission well above autofluorescence levels at non-toxic

43

concentrations. *In vitro* imaging studies show that both nanomaterials are successfully internalized with peak treatment times of 1 hour for GO; 12 hours for GQDs, with successive excretion. Lastly, graphene oxide appeared to localize primarily with the lysosomes during the colocalization study. This suggests cellular entry through endocytosis. As a result, we infer that both GO and GQDs can be used for image-guided delivery with tracking in the visible and also in the near-IR for GQDs, suggesting their further potential for *in vivo* imaging.

iii.   Do they offer sensing capabilities?

Based on its pH-dependent emission spectra, GO can be used as a ratiometric detection tool of acidic cancerous microenvironments proved to be effective in vitro. Magnitudes of the green to red GO emission ratios used to assess acidic versus regular biological pH show substantial variation for extracellular healthy versus cancer environments for three cell lines, allowing for differentiation between those. The spectra for NS-GQDs and N-GQDs suggest that they too can be used to sense a difference in pH between acidic cancerous and regular healthy environments. BN-GQDs do not show the same result, and therefore cannot be used as a sensing agent. When introduced to cancer versus healthy cell cultures, NS-GQDs and N-GQDs show even more significant difference in their green to blue emission ratios associated with the acidity of the environment. This way they allow to distinguish between acidic and regular environments in cancer and healthy extracellular regions. Therefore, it is concluded that GO and GQDs in general do offer sensing capabilities for biomedical applications.

5.3 Future Works

Our next step will be a two-step process where we will combine our tested nanomaterials-based delivery agents with anticancer drugs and genes, including doxorubicin, gemcitabine, paclitaxel and siRNA[133, 134] and then test their efficacy *in vitro*. We will study the effect of using combinations of genes and drugs delivered concomitantly by the nanocarriers as those are known to produce significantly improved anticancer effect [135, 136, 137]. The objective is to create an innovative treatment formulation that allows us to image *in vitro*, sense a difference within a cellular environment, and deliver an anticancer agent/gene therapy to a cell via a nanovehicle.

Upon attachment of cancer therapeutic or siRNA gene therapy agents, we will repeat previous steps to assess how different cell types react to the different formulations. While additional research must be done for each formulation, we can hypothesize effective attachment via non-covalent interactions. This is the simplest way to attach the drug while providing a capability of easy clearance of the therapeutic once it enters the cell. If this turns out to not be a possibility, we could consider chemical linkage from functional groups of graphene oxide and GQDs including epoxy, carbonyl hydroxy and carboxyl groups. We may also covalently attach, cancer-targeting agents such as hyaluronic acid[138] or tumor-targeting peptides[139] in collaboration with the Department of Chemistry and Biochemistry at TCU.

We will assess the efficacy of our therapies when delivered by nanomaterials alone and in combination. For drugs, we will begin by testing for toxicity within the cells, whereas for gene therapies we will test knockdown. If the results are consistent with our hypothesis, we will continue on to test these formulations *in vivo*. pH analysis, internalization/excretion analysis, and imaging studies will be repeated, and the results will be compared to those of the initial nanomaterial experiments. This allows us to determine the efficacy of the treatment formulations. We will

compare cytotoxicity/knockdown, imaging fluorescent intensities, and sensing capabilities. Upon the analysis, the most effective formulations will be selected for the use in animal studies.

Prior to further animal work we would like to verify the capability of cancer detection via GQD near-IR emission that has a potential to be used *in vivo* due to its higher tissue penetration. The next step is to test the treatment formulations *in vivo*, and determine which formulation provides the most effective multimodal agent. It is critical to test the functionality of the treatment formulation *in vi*vo, as this is where current nanoparticles often fall short of revolutionizing treatment plans. We will first conduct a toxicity study with our formulation with less expensive BL-6 mice testing the maximum dose to be administered. Further we will treat tumor-bearing mice with subcutaneous tumors. The study will test the following groups for each formulation: non-treatment control, therapeutic alone, nanomaterial vehicle control, and the combination of these, referred to as the treatment formulation. The efficacy of the formulation will be assessed via measuring tumor volume with a caliper. Finally, we will test the organ tissues in a bio-distribution study with BL-6 mice imaging the presence of the therapeutic formulation and assessing its sensing capabilities and its efficacy in organs including liver, spleen, kidneys and tumor via near-IR part of the intrinsic fluorescence of the nanomaterials. On the basis of these analyses, we will select the most efficacious formulation.

Optical properties will be explored, allowing for the determination of optimal imaging settings. Sensing capabilities will be investigated for quantum dots, along with other graphene derivatives, to determine the optimal settings for imaging in organ slices. As a result, the optimized animal-tested formulation is expected to provide conclusive evidence of the efficacy of our drug-nanoparticle treatment formulation. An *in vivo* study provides more information as to how the formulation would hold up as a treatment formulation for human patients. Successful results,

analyzed using the methods and assessments listed below, could improve cancer treatment and diagnostics, as well as improving the efficacy of treatment of a number of diseases/conditions with a variety of payloads delivered via an innovative multifunctional nanomaterials-based approach.

REFERENCES:

1   Wu, Z.-S. *et al.* Synthesis of Graphene Sheets with High Electrical Conductivity and Good Thermal Stability by Hydrogen Arc Discharge Exfoliation. doi:10.1021/nn900020u (2009).
2   Ghosh, S. *et al.* Extremely high thermal conductivity of graphene: Prospects for thermal management applications in nanoelectronic circuits. doi:L08-01858FIX-NO (2008).
3   Rafiee, M. A. *et al.* Fracture and Fatigue in Graphene Nanocomposites - Rafiee - 2010 - Small - Wiley Online Library. doi:10.1002/smll.200901480 (2010).
4   Nair, R. R. *et al.* Fine Structure Constant Defines Visual Transparency of Graphene. doi:10.1126/science.1156965 (2008).
5   Martin, N., Ros, T. D. & Nierengarten, J.-F. Carbon nanostructures in biology and medicine. doi:10.1039/C7TB90108A (2017).
6   Eda, G. *et al.* Blue photoluminescence from chemically derived graphene oxide. *Advanced materials (Deerfield Beach, Fla.)* **22**, 505-509, doi:10.1002/adma.200901996 (2010).
7   Cancer statistics, 2018 - Siegel - 2018 - CA: A Cancer Journal for Clinicians - Wiley Online Library. doi:10.3322/caac.21442 (2018).
8   Peer, D. *et al.* Nanocarriers as an emerging platform for cancer therapy. *Nature Nanotechnology* **2**, 751, doi:doi:10.1038/nnano.2007.387 (2007).
9   Fernandez-Fernandez, A., Manchanda, R. & McGoron, A. J. Theranostic Applications of Nanomaterials in Cancer: Drug Delivery, Image-Guided Therapy, and Multifunctional Platforms | SpringerLink. doi:10.1007/s12010-011-9383-z (2011).
10   Niu, C., Song, Q., He, G., Na, N. & Ouyang, J. Near-Infrared-Fluorescent Probes for Bioapplications Based on Silica-Coated Gold Nanobipyramids with Distance-Dependent Plasmon-Enhanced Fluorescence. *Analytical chemistry* **88**, 11062-11069, doi:10.1021/acs.analchem.6b03034 (2016).
11   Nanoscale imaging and sensing for biomedical applications - Fixler - 2017 - Cytometry Part A - Wiley Online Library. doi:10.1002/cyto.a.23188 (2018).
12   Sekar, R. B. & Periasamy, A. in *J Cell Biol* Vol. 160   629-633 (2003).
13   Shrestha, D., Jenei, A., Nagy, P., Vereb, G. & Szöllősi, J. in *Int J Mol Sci* Vol. 16   6718-6756 (2015).
14   Benninger, R. K. & Piston, D. W. Two-Photon Excitation Microscopy for the Study of Living Cells and Tissues. *Curr Protoc Cell Biol* **0 4**, Unit-4 1124, doi:10.1002/0471143030.cb0411s59 (2013).
15   Haley, B., barbara.haley@utsouthwestern.edu & Frenkel, E. Nanoparticles for drug delivery in cancer treatment. *Urologic Oncology: Seminars and Original Investigations* **26**, 57-64, doi:10.1016/j.urolonc.2007.03.015 (2008).
16   Srikanth, M. & Kessler, J. A. Nanotechnology—novel therapeutics for CNS disorders. *Nat Rev Neurol* **8**, 307-318, doi:10.1038/nrneurol.2012.76.
17   Kumar, M., Guo, Y. & Zhang, P. Highly sensitive and selective oligonucleotide sensor for sickle cell disease gene using photon upconverting nanoparticles. *Biosensors and Bioelectronics* **24**, 1522-1526, doi:https://doi.org/10.1016/j.bios.2008.08.023 (2009).
18   Zolnik, B. S., González-Fernández, Á., Sadrieh, N. & Dobrovolskaia, M. A. in *Endocrinology* Vol. 151   458-465 (2010).
19   Markiewski, M. M. *et al.* Modulation of the anti-tumor immune response by complement. *Nat Immunol* **9**, 1225-1235, doi:10.1038/ni.1655 (2008).
20   Mitchell, L. A., Lauer, F. T., Burchiel, S. W. & McDonald, J. D. Mechanisms for how Inhaled Multiwalled Carbon Nanotubes Suppress Systemic Immune Function in Mice. *Nat Nanotechnol* **4**, 451-456, doi:10.1038/nnano.2009.151 (2009).
21   Cai, W., Gao, T., Hong, H. & Sun, J. in *Nanotechnol Sci Appl* Vol. 1   17-32 (2008).
22   Qin, W. *et al.* Biocompatible Nanoparticles with Aggregation-Induced Emission Characteristics as Far-Red/Near-Infrared Fluorescent Bioprobes for In Vitro and In Vivo Imaging Applications -

Qin - 2012 - Advanced Functional Materials - Wiley Online Library. doi:10.1002/adfm.201102191 (2011).

23   Li, S.-D., Chen, Y.-C., Hackett, M. J. & Huang, L. Tumor-targeted Delivery of siRNA by Self-assembled Nanoparticles. *Molecular Therapy* **16**, 163-169, doi:https://doi.org/10.1038/sj.mt.6300323 (2008).

24   Cheng, J. *et al.* Formulation of functionalized PLGA–PEG nanoparticles for in vivo targeted drug delivery. *Biomaterials* **28**, 869-876, doi:https://doi.org/10.1016/j.biomaterials.2006.09.047 (2007).

25   Multifunctional pH-sensitive magnetic nanoparticles for simultaneous imaging, sensing and targeted intracellular anticancer drug delivery - IOPscience. doi:doi:10.1088/0957-4484/19/50/505104 (2008).

26   Sanvicens, N. & Marco, M. P. Multifunctional nanoparticles – properties and prospects for their use in human medicine. *Trends in biotechnology* **26**, 425-433, doi:https://doi.org/10.1016/j.tibtech.2008.04.005 (2008).

27   Chen, M.-L., He, Y.-J., Chen, X.-W. & Wang, J.-H. Quantum-Dot-Conjugated Graphene as a Probe for Simultaneous Cancer-Targeted Fluorescent Imaging, Tracking, and Monitoring Drug Delivery. doi:10.1021/bc3004809 (2013).

28   Blanco, E., Shen, H. & Ferrari, M. Principles of nanoparticle design for overcoming biological barriers to drug delivery. *Nature Biotechnology* **33**, 941, doi:doi:10.1038/nbt.3330 (2015).

29   Rieter, W. J., Pott, K. M., Taylor, K. M. L. & Lin, W. Nanoscale Coordination Polymers for Platinum-Based Anticancer Drug Delivery. doi:10.1021/ja803383k (2008).

30   Conjugation of quantum dots with graphene for fluorescence imaging of live cells. doi:10.1039/C1AN15474E (2011).

31   Kirkpatrick, D. L. *et al.* in *Materials (Basel)* Vol. 5   278-301 (2012).

32   Cohen-Tanugi, D. & Grossman, J. C. Water Desalination across Nanoporous Graphene. doi:10.1021/nl3012853 (2012).

33   Schwierz, F. Graphene transistors. *Nature Nanotechnology* **5**, 487-496, doi:doi:10.1038/nnano.2010.89 (2010).

34   Randviir, E. P., Brownson, D. A. C. & Banks, C. E. A decade of graphene research: production, applications and outlook. *Materials Today* **17**, 426-432, doi:https://doi.org/10.1016/j.mattod.2014.06.001 (2014).

35   Kim, Y.-K. & Min, D.-H. Preparation of the Hybrid Film of Poly(allylamine hydrochloride)-Functionalized Graphene Oxide and Gold Nanoparticle and Its Application for Laser-Induced Desorption/Ionization of Small Molecules. doi:10.1021/la204185p (2012).

36   Yuk, J. M. *et al.* High-Resolution EM of Colloidal Nanocrystal Growth Using Graphene Liquid Cells. doi:10.1126/science.1217654 (2012).

37   Min, S. K., Kim, W. Y., Cho, Y. & Kim, K. S. Fast DNA sequencing with a graphene-based nanochannel device. *Nature Nanotechnology* **6**, 162-165, doi:doi:10.1038/nnano.2010.283 (2011).

38   Wang, Y., Li, Z., Wang, J., Li, J. & Lin, Y. Graphene and graphene oxide: biofunctionalization and applications in biotechnology. *Trends in biotechnology* **29**, 205-212, doi:10.1016/j.tibtech.2011.01.008 (2011).

39   Si, Y. & Samulski, E. T. Synthesis of Water Soluble Graphene. doi:10.1021/nl080604h (2008).

40   Peng, C., Hu, W., Zhou, Y., Fan, C. & Huang, Q. Intracellular Imaging with a Graphene-Based Fluorescent Probe - Peng - 2010 - Small - Wiley Online Library. doi:10.1002/smll.201000560 (2010).

41   Naumov, E. C. M. T. H. C. P. K. C. G. R. A. A. V. *Graphene Oxide as a Multifunctional Platform for Intracellular Delivery, Imaging, and Cancer Sensing* (in press).

42   A Review on Graphene-Based Nanomaterials in Biomedical Applications and Risks in Environment and Health | SpringerLink. doi:10.1007/s40820-018-0206-4 (2018).

43   Qu, Y. *et al.*   (2018).

44   Cheng, J. *et al.* Formulation of functionalized PLGA-PEG nanoparticles for in vivo targeted drug delivery. *Biomaterials* **28**, 869-876, doi:10.1016/j.biomaterials.2006.09.047 (2007).

45   Vaishali Bagalkot, ‡ *et al.* Quantum Dot−Aptamer Conjugates for Synchronous Cancer Imaging, Therapy, and Sensing of Drug Delivery Based on Bi-Fluorescence Resonance Energy Transfer. doi:S1530-6984(07)01546-9 (2007).

46   Kim, D., Jeong, Y. Y. & Jon, S. A Drug-Loaded Aptamer−Gold Nanoparticle Bioconjugate for Combined CT Imaging and Therapy of Prostate Cancer. doi:10.1021/nn901877h (2010).

47   Fabrication of Water-Dispersible Polyaniline-Poly(4-styrenesulfonate) Nanoparticles For Inkjet-Printed Chemical-Sensor Applications - Jang - 2007 - Advanced Materials - Wiley Online Library. doi:10.1002/adma.200602127 (2007).

48   Jokerst, J. V., Lobovkina, T., Zare, R. N. & Gambhir, S. S. Nanoparticle PEGylation for imaging and therapy. *Nanomedicine (Lond)* **6**, 715-728, doi:10.2217/nnm.11.19 (2011).

49   Bae, Y. H. & Park, K. Targeted drug delivery to tumors: Myths, reality and possibility. *J Control Release* **153**, 198-205, doi:10.1016/j.jconrel.2011.06.001 (2011).

50   Chang, H., Tang, L., Wang, Y., Jiang, J. & Li, J. Graphene Fluorescence Resonance Energy Transfer Aptasensor for the Thrombin Detection. doi:10.1021/ac9025384 (2010).

51   Karchemski, F., Zucker, D., Barenholz, Y. & Regev, O. Carbon nanotubes-liposomes conjugate as a platform for drug delivery into cells. *Journal of Controlled Release* **160**, 339-345, doi:https://doi.org/10.1016/j.jconrel.2011.12.037 (2012).

52   Zhang, M. *et al.* Facile synthesis of water-soluble, highly fluorescent graphene quantum dots as a robust biological label for stem cells. doi:10.1039/C2JM16835A (2012).

53   A graphene oxide -based fluorescent aptasensor for the turn-on detection of epithelial tumor marker mucin 1. doi:10.1039/C2NR12061E (2012).

54   A nanoscale graphene oxide– peptide biosensor for real-time specific biomarker detection on the cell surface. doi:10.1039/C2CC31974H (2012).

55   Chung, C. *et al.* Biomedical applications of graphene and graphene oxide. *Accounts of chemical research* **46**, 2211-2224, doi:10.1021/ar300159f (2013).

56   Pumera, M. Graphene in biosensing. *ScienceDirect* **14**, 308-315, doi:10.1016/S1369-7021(11)70160-2 (2011).

57   Feng, L. *et al.* New Horizons for Diagnostics and Therapeutic Applications of Graphene and Graphene Oxide. *Advanced Materials* **25**, 168-186, doi:10.1002/adma.201203229 (2017).

58   Wang, Y. *et al.* Aptamer/Graphene Oxide Nanocomplex for in Situ Molecular Probing in Living Cells. doi:10.1021/ja103169v (2010).

59   Shen, H., Zhang, L., Liu, M. & Zhang, Z. in *Theranostics* Vol. 2   283-294 (2012).

60   Jung, H. S. *et al.* Nanographene Oxide–Hyaluronic Acid Conjugate for Photothermal Ablation Therapy of Skin Cancer. doi:10.1021/nn405383a (2014).

61   Sun, X. *et al.* Nano-Graphene Oxide for Cellular Imaging and Drug Delivery. *Nano Res* **1**, 203-212, doi:10.1007/s12274-008-8021-8 (2008).

62   Graphene based materials for biomedical applications - ScienceDirect. doi:10.1016/j.mattod.2013.09.004 (2017).

63   Feng, L., Zhang, S. & Liu, Z. Graphene based gene transfection. doi:10.1039/C0NR00680G (2011).

64   Lu, C.-H. *et al.* Using graphene to protect DNA from cleavage during cellular delivery. doi:10.1039/B926893F (2010).

65   Zhang, C. *et al.* Biosensing Platform Based on Fluorescence Resonance Energy Transfer from Upconverting Nanocrystals to Graphene Oxide. *Angewandte Chemie International Edition* **50**, 6851-6854, doi:10.1002/anie.201100769 (2011).

66   Novoselov, K. S. *et al.* A roadmap for graphene. *Nature* **490**, 192, doi:doi:10.1038/nature11458 (2012).

67   Yang, K., Feng, L., Shi, X. & Liu, Z. Nano-graphene in biomedicine: theranostic applications. doi:10.1039/C2CS35342C (2012).

68   Pramanik, A. *et al.* Extremely High Two-Photon Absorbing Graphene Oxide for Imaging of Tumor Cells in the Second Biological Window. doi:10.1021/jz5009856 (2014).

69   Gonzalez-Rodriguez, R., Granitzer, P., Rumpf, K. & Coffer, J. L. New MRI contrast agents based on silicon nanotubes loaded with superparamagnetic iron oxide nanoparticles. doi:10.1098/rsos.180697 (2018).

70   Galande, C. *et al.* Quasi-Molecular Fluorescence from Graphene Oxide. *Scientific Reports* **1**, 85, doi:doi:10.1038/srep00085 (2011).

71   Frontiers | Lactate Contribution to the Tumor Microenvironment: Mechanisms, Effects on Immune Cells and Therapeutic Relevance | Immunology. doi:doi:10.3389/fimmu.2016.00052 (2016).

72   Galande, C. *et al.* Quasi-Molecular Fluorescence from Graphene Oxide. *Scientific Reports* **1**, doi:doi:10.1038/srep00085 (2011).

73   Hummers, W. S. & Offeman, R. E. Preparation of Graphitic Oxide. *Journal of the American Chemical Society*, doi:10.1021/ja01539a017 (1958).

74   Liu, Z., Robinson, J. T., Sun, X. & Dai, H. PEGylated Nanographene Oxide for Delivery of Water-Insoluble Cancer Drugs. doi:10.1021/ja803688x (2008).

75   Imani, R. *et al.* Dual-functionalized graphene oxide for enhanced siRNA delivery to breast cancer cells - ScienceDirect. **147**, doi:10.1016/j.colsurfb.2016.08.015 (2016).

76   Feng Yin, K. H., Yangzi Chen, Mengying Yu, Dongyuan Wang, Qianqian Wang, Ken-Tye Yong, Fei Lu, Yongye Liang, Zigang Li. SiRNA Delivery with PEGylated Graphene Oxide Nanosheets for Combined Photothermal and Genetherapy for Pancreatic Cancer [Abstract]. *Theranostics* (2017).

77   Ren, L., Zhang, Y., Cui, C., Bi, Y. & Ge, X. Functionalized graphene oxide for anti-VEGF siRNA delivery: preparation, characterization and evaluation in vitro and in vivo. doi:10.1039/C7RA00810D (2017).

78   Liu, Q., Guo, B., Rao, Z., Zhang, B. & Gong, J. R. Strong Two-Photon-Induced Fluorescence from Photostable, Biocompatible Nitrogen-Doped Graphene Quantum Dots for Cellular and Deep-Tissue Imaging. doi:10.1021/nl400368v (2013).

79   Markovic, Z. M. *et al.* Graphene quantum dots as autophagy-inducing photodynamic agents. *Biomaterials* **33**, 7084-7092, doi:https://doi.org/10.1016/j.biomaterials.2012.06.060 (2012).

80   Dong, Y. *et al.* Carbon-Based Dots Co-doped with Nitrogen and Sulfur for High Quantum Yield and Excitation-Independent Emission - Dong - 2013 - Angewandte Chemie International Edition - Wiley Online Library. doi:10.1002/anie.201301114 (2013).

81   Michalet, X. *et al.* Quantum Dots for Live Cells, in Vivo Imaging, and Diagnostics. doi:10.1126/science.1104274 (2005).

82   Ya-Ping Sun *et al.* Quantum-Sized Carbon Dots for Bright and Colorful Photoluminescence. doi:S0002-7863(06)02677-1 (2006).

83   Smith, A. M., Mancini, M. C. & Nie, S. Second window for in vivo imaging. *Nat Nanotechnol* **4**, 710-711, doi:10.1038/nnano.2009.326 (2009).

84   Three Colors Emission from S,N Co-doped Graphene Quantum Dots for Visible Light H2 Production and Bioimaging - Qu - 2015 - Advanced Optical Materials - Wiley Online Library. doi:10.1002/adom.201400549 (2015).

85   Photo-and Electroluminescence from Nitrogen-Doped and Nitrogen–Sulfur Codoped Graphene Quantum Dots - Hasan - - Advanced Functional Materials - Wiley Online Library. doi:10.1002/adfm.201804337 (2018).

86   Sun, H., Wu, L., Gao, N., Ren, J. & Qu, X. Improvement of Photoluminescence of Graphene Quantum Dots with a Biocompatible Photochemical Reduction Pathway and Its Bioimaging Application. doi:10.1021/am3030849 (2013).

87   Kim, S. *et al.* Near-infrared fluorescent type II quantum dots for sentinel lymph node mapping. *Nat Biotechnol* **22**, 93-97, doi:10.1038/nbt920 (2004).

88   Kozawa, D. *et al.* Excitonic Photoluminescence from Nanodisc States in Graphene Oxides. doi:10.1021/jz500516u (2014).

89   Gokus, T. *et al.* Making Graphene Luminescent by Oxygen Plasma Treatment. doi:10.1021/nn9012753 (2009).

90   Cuong, T. V. *et al.* Temperature-dependent photoluminescence from chemically and thermally reduced graphene oxide. doi:L11-05611R (2011).

91   Hasan, M. T. *et al.* Optical Band Gap Alteration of Graphene Oxide via Ozone Treatment. *Scientific Reports* **7**, 6411, doi:doi:10.1038/s41598-017-06107-0 (2017).

92   Loh, K. P., Bao, Q., Eda, G. & Chhowalla, M. Graphene oxide as a chemically tunable platform for optical applications. *Nature Chemistry* **2**, 1015, doi:doi:10.1038/nchem.907 (2010).

93   Krishnamoorthy, K., Veerapandian, M., Yun, K. & S.-J.Kim. The chemical and structural analysis of graphene oxide with different degrees of oxidation - ScienceDirect. *Elsevier* **53**, doi:10.1016/j.carbon.2012.10.013 (2013).

94   Zhu, Y. *et al.* Graphene and Graphene Oxide: Synthesis, Properties, and Applications. *Advanced Materials* **22**, 3906-3924, doi:10.1002/adma.201001068 (2017).

95   Eigler, S. *Graphene oxide : fundamentals and applications*. (Wiley, 2017).

96   Jiang, W., Kim, B. Y. S., Rutka, J. T. & Chan, W. C. W. Nanoparticle-mediated cellular response is size-dependent. *Nature Nanotechnology* **3**, 145-150, doi:doi:10.1038/nnano.2008.30 (2008).

97   Hanene, A.-B. *et al.* Purified Graphene Oxide Dispersions Lack In Vitro Cytotoxicity and In Vivo Pathogenicity. *Advanced Healthcare Materials* **2**, 433-441, doi:doi:10.1002/adhm.201200248 (2013).

98   Harrison, B. S. & Atala, A. Carbon nanotube applications for tissue engineering. *Biomaterials* **28**, 344-353, doi:https://doi.org/10.1016/j.biomaterials.2006.07.044 (2007).

99   Arnaud Magrez, † *et al.* Cellular Toxicity of Carbon-Based Nanomaterials. doi:S1530-6984(06)00162-7 (2006).

100   Highly efficient photoluminescent graphene oxide with tunable surface properties. doi:10.1039/C0CC02374D (2010).

101   Kato, Y. *et al.* Acidic extracellular microenvironment and cancer. *Cancer Cell International* **13**, 89, doi:10.1186/1475-2867-13-89 (2013).

102   Alberts, B. *et al.* Looking at the Structure of Cells in the Microscope. doi:https://www.ncbi.nlm.nih.gov/books/NBK26880/ (2002).

103   Mei, Q. *et al.* Highly efficient photoluminescent graphene oxide with tunable surface properties. doi:10.1039/C0CC02374D (2010).

104   Gratton, S. E. A. *et al.* The effect of particle design on cellular internalization pathways. doi:10.1073/pnas.0801763105 (2008).

105   Cho, K., Wang, X., Nie, S., Chen, Z. G. & Shin, D. M. Therapeutic Nanoparticles for Drug Delivery in Cancer. doi:10.1158/1078-0432.CCR-07-1441 (2008).

106   Dunn, K. W., Kamocka, M. M. & McDonald, J. H. in *Am J Physiol Cell Physiol* Vol. 300 C723-742 (2011).

107   Cellular Uptake, Intracellular Trafficking, and Cytotoxicity of Nanomaterials - Zhao - 2011 - Small - Wiley Online Library. doi:10.1002/smll.201100001 (2011).

108   Romero-Garcia, S., Moreno-Altamirano, M. M. B., Prado-Garcia, H. & Sánchez-García, F. J. Lactate Contribution to the Tumor Microenvironment: Mechanisms, Effects on Immune Cells and Therapeutic Relevance. *Front Immunol* **7**, doi:10.3389/fimmu.2016.00052 (2016).

109   Swietach, P., Vaughan-Jones, R. D., Harris, A. L. & Hulikova, A. in *Philos Trans R Soc Lond B Biol Sci* Vol. 369   (2014).

110   Gerweck, L. E. & Seetharaman, K. Cellular pH Gradient in Tumor versus Normal Tissue: Potential Exploitation for the Treatment of Cancer. (1996).

111   Lodish, B., Kaiser, Krieger, Scott, Bratscher, Ploegh, Matsudaira. *Molecular Cell Biology*. 6 edn, (2008).

112   Casey, J. R., Grinstein, S. & Orlowski, J. Sensors and regulators of intracellular pH. *Nature Reviews Molecular Cell Biology* **11**, 50-61, doi:doi:10.1038/nrm2820 (2009).

113   Damaghi, M., Wojtkowiak, J. W. & Gillies, R. J. pH sensing and regulation in cancer. *Front Physiol* **4**, doi:10.3389/fphys.2013.00370 (2013).

114   Chou, S. S. *et al.* Nanoscale Graphene Oxide (nGO) as Artificial Receptors: Implications for Biomolecular Interactions and Sensing. doi:10.1021/ja306767y (2012).

115   Farzaneh, F. *et al.* in *Asian Pac J Cancer Prev* Vol. 18   431-435 (2017).

116   Chen, S. *et al.* Full-Range Intracellular pH Sensing by an Aggregation-Induced Emission-Active Two-Channel Ratiometric Fluorogen. doi:10.1021/ja400337p (2013).

117   Zong, S., Wang, Z., Yang, J. & Cui, Y. Intracellular pH Sensing Using p-Aminothiophenol Functionalized Gold Nanorods with Low Cytotoxicity. doi:10.1021/ac200467z (2011).

118   Asati, A., Kaittanis, C., Santra, S. & Perez, J. M. pH-Tunable Oxidase-Like Activity of Cerium Oxide Nanoparticles Achieving Sensitive Fluorigenic Detection of Cancer Biomarkers at Neutral pH. doi:10.1021/ac102826k (2011).

119   Akira Matsumoto, Syuhei Ikeda, Atsushi Harada, a. & Kataoka*, K. Glucose-Responsive Polymer Bearing a Novel Phenylborate Derivative as a Glucose-Sensing Moiety Operating at Physiological pH Conditions. doi:S1525-7797(03)04139-4 (2003).

120   Recent advances in fluorescent nucleic acid probes for living cell studies. doi:10.1039/C2AN35254K (2012).

121   Antaris, A. L. *et al.* Ultra-Low Doses of Chirality Sorted (6,5) Carbon Nanotubes for Simultaneous Tumor Imaging and Photothermal Therapy. doi:10.1021/nn4006472 (2013).

122   Kukowska-Latallo, J. F. *et al.* Nanoparticle Targeting of Anticancer Drug Improves Therapeutic Response in Animal Model of Human Epithelial Cancer. doi:10.1158/0008-5472.CAN-04-3921 (2005).

123   Graphene quantum dots : emergent nanolights for bioimaging, sensors, catalysis and photovoltaic devices. doi:10.1039/C2CC00110A (2012).

124   Frasco, M. & Chaniotakis, N. Semiconductor Quantum Dots in Chemical Sensors and Biosensors. *Sensors* **9**, 7266-7286, doi:10.3390/s90907266 (2009).

125   Fabrication of highly fluorescent graphene quantum dots using l-glutamic acid for in vitro / in vivo imaging and sensing. doi:10.1039/C3TC30820K (2013).

126   Hasan, M. T. Enhancing the Power Conversion Efficiency of Solar Cells using Ozone-Oxidized Nitrogen Doped Graphene Quantum Dots. (in preparation).

127   Cetinel, S. & Montemagno, C. Nanotechnology Applications for Glaucoma. *Asia-Pacific journal of ophthalmology (Philadelphia, Pa.)* **5**, 70-78, doi:10.1097/apo.0000000000000171 (2016).

128   Jiang, S., Franco, Y. L., Zhou, Y. & Chen, J. in *Int J Ophthalmol* Vol. 11   1038-1044 (2018).

129   Weng, Y. *et al.* Nanotechnology-based strategies for treatment of ocular disease. *Acta Pharmaceutica Sinica B* **7**, 281-291, doi:https://doi.org/10.1016/j.apsb.2016.09.001 (2017).

130   Hawkins, B. T. & Davis, T. P. The Blood-Brain Barrier/Neurovascular Unit in Health and Disease. doi:10.1124/pr.57.2.4 (2005).

131   Tsai, Y.-M., Chien, C.-F., Lin, L.-C. & Tsai, T.-H. Curcumin and its nano-formulation: The kinetics of tissue distribution and blood–brain barrier penetration. *International Journal of Pharmaceutics* **416**, 331-338, doi:https://doi.org/10.1016/j.ijpharm.2011.06.030 (2011).

132   Hamblin, M. R. Shining light on the head: Photobiomodulation for brain disorders. *BBA Clinical* **6**, 113-124, doi:https://doi.org/10.1016/j.bbacli.2016.09.002 (2016).

133   Zhang, L., Xia, J., Zhao, Q., Liu, L. & Zhang, Z. Functional Graphene Oxide as a Nanocarrier for Controlled Loading and Targeted Delivery of Mixed Anticancer Drugs - Zhang - 2010 - Small - Wiley Online Library. doi:10.1002/smll.200901680 (2010).

134   Ihle, N. T. *et al.* Molecular pharmacology and antitumor activity of PX-866, a novel inhibitor of phosphoinositide-3-kinase signaling. (2004).

135   Wiradharma, N., Tong, Y. W. & Yang, Y.-Y. Self-assembled oligopeptide nanostructures for co-delivery of drug and gene with synergistic therapeutic effect. *Biomaterials* **30**, 3100-3109, doi:https://doi.org/10.1016/j.biomaterials.2009.03.006 (2009).

136   Liu, Y., Miyoshi, H. & Nakamura, M. Nanomedicine for drug delivery and imaging: A promising avenue for cancer therapy and diagnosis using targeted functional nanoparticles - Liu - 2007 - International Journal of Cancer - Wiley Online Library. doi:10.1002/ijc.22709 (2007).

137   Sun, D. T. *et al.* Engineered Nanoparticles for Drug Delivery in Cancer Therapy - Sun - 2014 - Angewandte Chemie International Edition - Wiley Online Library. doi:10.1002/anie.201403036 (2014).

138   Jiang, T. *et al.* Dual-functional liposomes based on pH-responsive cell-penetrating peptide and hyaluronic acid for tumor-targeted anticancer drug delivery. *Biomaterials* **33**, 9246-9258, doi:https://doi.org/10.1016/j.biomaterials.2012.09.027 (2012).

139   Landon, L. A. & Deutscher, S. L. Combinatorial discovery of tumor targeting peptides using phage display - Landon - 2003 - Journal of Cellular Biochemistry - Wiley Online Library. doi:10.1002/jcb.10634 (2003).

VITA

PERSONAL

Elizabeth Campbell
Fort Worth, Texas

EDUCATION

2016-Present
Texas Christian University, Department of Physics and Astronomy
Graduate Student

2010-2014
University of Dallas, Irving, Texas
Department of Physics
Bachelor of Science in Physics

PROFESSIONAL EXPERIENCE

2016-Present   Graduate Teaching Assistant, Texas Christian University

2014-2016   Teacher, Fort Worth ISD

PUBLICATIONS

1. *Afeefah Khazi-Syed, Md. Tanvir Hasan,* **E. Campbell***, Anton V. Naumov* "Single-Walled Carbon Nanotube-Assisted Antibiotic Delivery and Imaging in S. Epidermidis Strains Addressing Antibiotic Resistance" under preparation (2018).

2. **E. Campbell***, Md. Tanvir Hasan, Christine Pho, K. Callaghan, G.R. Akkaraju, and Anton V. Naumov* "Graphene Oxide as a Multifunctional Platform for Intracellular Delivery, Imaging, and Cancer Sensing" Nature Scientific Reports, doi: 10.1038/s41598-018-36617-4 (2018).

3. *Roberto Gonzalez-Rodriguez,* **Elizabeth Campbell***, Anton Naumov* "Multifunctional Graphene oxide/Iron oxide Nanoparticles for Magnetic Targeted Drug Delivery Dual Magnetic Resonance/Fluorescence Imaging and Cancer Sensing" submitted to PLOS One (2018).

ABSTRACT

CARBON NANOMATERIALS AS IMAGING, SENSING, AND DELIVERY AGENTS FOR
CANCER THERAPEUTICS

By: Elizabeth Campbell, M.S., 2018
Department of Physics & Astronomy
Texas Christian University

Advisor: Anton V. Naumov, Assistant Professor of Physics

The objective of this research is to develop, optimize and test graphene quantum dots (GQDs) and graphene oxide (GO) for imaging, sensing, and drug delivery. GO and GQDs both possess properties beneficial for molecular drug delivery/imaging/sensing applications. GO exhibits pH-dependent fluorescence in the visible tailing into near-infrared, is water soluble and has a substantial platform for functionalization with multiple therapeutics. GQDs are beneficial for their biocompatibility, small size (< 5 nm), ease in synthesis, and high yield fluorescence in the visible and near-infrared. We explore the imaging and sensing capabilities of GO and GQDs *in vitro* via their intrinsic fluorescence, pH-dependence of their emission for detection of acidic cancerous environments, and capabilities for *in vitro* transport of therapeutics. As a result, we expect GO and GQDs to introduce a new paradigm, becoming multi-functional agents for imaging, sensing, and drug delivery advancing scientific approach to cancer treatment and therapeutics.